ASSESSING TARGET SPECIFICITY OF THE SMALL MOLECULE INHIBITOR MARIMASTAT TO SNAKE VENOM TOXINS: A NOVEL APPLICATION OF THERMAL PROTEOME PROFILING

Cara F. Smith[1], Cassandra M. Modahl[2], David Ceja-Galindo[1], Keira Y. Larson[1], Sean P. Maroney[1], Lilyrose Bahrabadi[1], Nicklaus P. Brandehoff[3], Blair W. Perry[4], Maxwell C. McCabe[1], Daniel Petras[5,6], Bruno Lomonte[7], Juan J. Calvete[8], Todd A. Castoe[9], Stephen P. Mackessy[10], Kirk C. Hansen[1], Anthony J. Saviola[1]

[1]Department of Biochemistry and Molecular Genetics, 12801 East 17th Avenue, University of Colorado Denver, Aurora, CO, USA

[2]Centre for Snakebite Research and Interventions, Liverpool School of Tropical Medicine, Pembroke Place, Liverpool, UK

[3]Rocky Mountain Poison and Drug Center, Denver Health and Hospital Authority, Denver, CO, USA

[4]School of Biological Sciences, Washington State University, Pullman, WA, USA

[5]CMFI Cluster of Excellence, University of Tuebingen, Tuebingen, Germany

[6] Department of Biochemistry, University of California Riverside, Riverside, CA, USA

[7]Instituto Clodomiro Picado, Facultad de Microbiología, Universidad de Costa Rica, San José, 11501-2060, Costa Rica

[8]Evolutionary and Translational Venomics Laboratory, Consejo Superior de Investigaciones Científicas (CSIC), 46010 Valencia, Spain

[9]Department of Biology, The University of Texas Arlington, Texas, USA

[10]Department of Biological Sciences, 501 20th Street, University of Northern Colorado, Greeley, CO 80639 USA

*Corresponding author: Anthony J. Saviola, Department of Biochemistry and Molecular Genetics, 12801 East 17th Avenue, University of Colorado Denver, Aurora, CO 80045 USA
Tel:303-724-3339. Email: Anthony.Saviola@cuanschutz.edu

Abstract

New treatments that circumvent the pitfalls of traditional antivenom therapies are critical to address the problem of snakebite globally. Numerous snake venom toxin inhibitors have shown promising cross-species neutralization of medically significant venom toxins *in vivo* and *in vitro*. The development of high-throughput approaches for the screening of such inhibitors could accelerate their identification, testing, and implementation, and thus holds exciting potential for improving the treatments and outcomes of snakebite envenomation worldwide. Energetics-based proteomic approaches, including Thermal Proteome Profiling (TPP) and Proteome Integral Solubility Alteration (PISA), assays represent "deep proteomics" methods for high throughput, proteome-wide identification of drug targets and ligands. In the following study, we apply TPP and PISA methods to characterize the interactions between venom toxin proteoforms in *Crotalus atrox* (Western Diamondback Rattlesnake) and the snake venom metalloprotease (SVMP) inhibitor marimastat. We investigate its venom proteome-wide effects and characterize its interactions with specific SVMP proteoforms, as well as its potential targeting of non-SVMP venom toxin families. We also compare the performance of PISA thermal window and soluble supernatant with insoluble precipitate using two inhibitor concentrations, providing the first demonstration of the utility of a sensitive high-throughput PISA-based approach to assess the direct targets of small molecule inhibitors for snake venom.

Introduction

Snakebite is a global public health problem that disproportionately affects impoverished communities in rural tropical and subtropical regions. Annual estimates suggest that snakebite affects 1.8–2.7 million people worldwide, causing >138,000 deaths and leaving an even larger number of victims suffering permanent disabilities (1), which has led to the designation of snakebite as a neglected tropical disease by the World Health Organization (WHO; 2,3). Snake venoms are complex toxic cocktails of proteins and peptides derived from more than a dozen gene families, many of which have undergone duplication to generate multiple functionally diverse paralogs and associated proteoforms in the venom of a single species (4–6). While substantial variation exists in the relative mass and functional activity of venom proteins and peptides, most of these toxins have evolved to target and disrupt numerous bodily systems (7–10). Adding to the complexity of snake venoms, the most medically relevant toxin families tend to be the most diverse with many paralogs and associated proteoforms displaying moderate-to-high sequence similarity but in many cases exhibiting a spectrum of distinct biological effects (7,9,11–13). One of these families, snake venom metalloproteases (SVMPs), is ubiquitous across snake species (but is particularly abundant in viperid venoms) and is responsible for many of the life-threatening pathologies that result from snake envenomation, including local and systemic hemorrhage, and tissue destruction (14–18).

The substantial morbidity and mortality resulting globally from snakebite may seem surprising considering that antivenoms (whole IgG molecules, Fab or $F(ab')_2$ fragments from venom-immunized animals) are often highly effective at recognizing and neutralizing the major toxic components of a venom (19,20). A major challenge to antivenom efficacy, however, is the significant variation in venom composition that occurs at phylogenetic (21–26), ontogenetic (27–

30), and geographic or population scales (31–36). As a consequence, antivenoms are most effective against the snake species whose venom was utilized during production and are often inadequate at recognizing venom components of different or even closely related snake species (25). Further, geographic venom variation may even result in poor neutralization within the same species when snakes used in antivenom production were sourced from a different location (33). Antivenoms also tend to be more effective at neutralizing systemic effects, but less effective at neutralizing anatomically localized manifestations of envenomation, which can result in permanent tissue damage and disfigurement (1,37–41). The storage, accessibility, and administration of antivenom also pose significant practical challenges in rural areas where it is needed most (10,37,42–48). These hurdles are further compounded by the excessive effort and cost of producing antivenoms for any one geographically-relevant set of venomous snake species.

While the use of polyvalent antivenoms has been the mainstay treatment for snake envenomation, the development of non-immunological treatments that circumvent the limitations of antivenoms has been prioritized as a goal to address the impacts of snake envenomation globally by the WHO (3). Recent applications of small molecule inhibitors against medically significant toxins have yielded promising preclinical results and these inhibitors have broad potential as supplemental therapies in combination with standard treatments (37,49–54). These inhibitors have a number of advantages over current antivenom therapies including better peripheral tissue distribution, higher shelf stability, a higher safety profile, the ability for pre-hospital oral or topical administration, and greater affordability (55). The use of novel high-throughput approaches for the testing of venom toxin inhibitors and the identification of their

112 targets could accelerate the implementation of effective small molecule inhibitors, with the long-
113 term potential of improving the treatment and outcome of snakebite envenomation globally.

114 Numerous studies have examined the effects of various small molecule inhibitors on the
115 biological activities of venoms *in vitro* and the neutralization capacity of these inhibitors *in vivo*
116 (49–51,53,56–59). A repurposed low-specificity matrix metalloprotease inhibitor, marimastat,
117 has shown effective neutralization of SVMP-rich venoms across multiple venomous snake
118 species by preventing both local and systemic toxicity (53), decreasing hemotoxic venom effects
119 (50,51,53,60,61), reducing SVMP-induced cytotoxicity (56,60), and inhibiting extracellular
120 matrix degradation (62). Because marimastat has previously progressed to clinical trials as a
121 cancer treatment, its safety profile has already been determined, accelerating its development as
122 a potential snakebite treatment (63,64). When administered with other small molecule inhibitors,
123 marimastat has shown *in vivo* neutralization of lethal toxicity and dermonecrosis in murine
124 models (50,56). Each of these studies assesses the downstream effects of inhibitor action *in vivo*
125 or *in vitro* by measuring changes to biological activity or survival; however, to our knowledge no
126 studies exist using a direct assessment of venom-wide target-ligand interactions between venom
127 toxins and small molecule inhibitors.

128 Thermal Proteome Profiling (TPP) is a prominent energetics-based proteomic approach
129 for identifying the molecular targets of drugs. TPP builds upon the concept that a protein's
130 physicochemical properties are altered through interactions with extrinsic factors (e.g., other
131 proteins, therapeutic drugs, metabolites) making it more or less resistant to thermal-induced
132 denaturation (65,66). Traditional TPP assays were centered on the principle that unbound
133 proteins tend to denature and become insoluble when subjected to increasing temperatures,
134 whereas proteins stabilized through interactions with extrinsic factors often exhibit increased

thermal stability and remain in solution (65,67–69). Identifying and quantifying such solubility changes via mass spectrometry can be used to infer direct or indirect interactions between a given compound and its protein targets (70).

Recently, the Proteome Integral Solubility Alteration (PISA) assay has emerged as a powerful strategy that retains the breadth and sensitivity of TPP but with a significant reduction in sample preparation and analysis time (70,71). PISA represents a “deep proteomics” method for high throughput proteome-wide target identification of ligands, with improved target discovery and higher statistical significance for target candidates (70–72). In a PISA assay, samples are subjected to heat across a temperature gradient (as in TPP) but are subsequently pooled prior to analysis (70,71). Rather than generating melt curves to determine exact melting temperatures, PISA compares overall abundance of each measured peptide between controls and treatments to detect differences in melting properties when a compound of interest is added. This methodology allows multiple variables to be altered simultaneously (e.g., concentration, temperature) in a high-throughput manner. It has recently been shown that heat-treating within a smaller temperature window can improve sensitivity and target discovery with PISA (73). TPP, PISA, and related methods derived from the same principles have been used to discover drug targets, antibiotic targets, and mechanisms of antibiotic resistance (65,66,69,74). In our specific context, these proteomic techniques applied to the development of envenomation treatments hold strong potential to provide rapid and high-throughput characterization of small molecule venom toxin inhibitors by determining their direct targets across diverse venom toxin protein families, accelerating identification of novel inhibitors.

Here, we apply TPP and PISA methods to characterize the physical interactions between the SVMP inhibitor marimastat and toxin proteoforms of *Crotalus atrox* (Western Diamondback

Rattlesnake) venom. First, we determined toxin proteoform presence and abundance in the venom of this well-studied species and used TPP to characterize the venom meltome by determining venom protein family-level and specific proteoform-level thermal characteristics. Next, we performed PISA experiments within two different thermal windows to assess protein thermal stability changes upon inhibitor addition to identify specific proteoform targets of the small molecule inhibitor marimastat. Because of the previously characterized differences in signal-to-noise ratio between supernatant and pellet in PISA experiments (75,76), we investigate and compare the targets identified in both the soluble and insoluble fractions. Our results demonstrate that a PISA-based approach can provide rapid, highly sensitive, and robust inferences for the unbiased proteome-wide screening of venom and inhibitor interactions.

Methods

Venom and inhibitors

Crotalus atrox (Western Diamondback rattlesnake) venom was obtained by manual extraction from snakes housed at the University of Northern Colorado (UNC) Animal Facility (Greeley, CO), in accordance with UNC-IACUC protocols. Venoms were lyophilized and stored at -20°C until use. Venoms were reconstituted at a concentration of 2 mg/mL and protein concentration was determined on a Nanodrop™ using the Absorbance 280 program. The small molecule matrix metalloprotease inhibitor marimastat ((2*S*,3*R*)-*N*4-[(1*S*)-2,2-Dimethyl-1-[(methylamino)carbonyl]propyl]-*N*1,2-dihydroxy-3-(2-methylpropyl)butanediamide, >98%, Cat no.: 2631, Tocris Bioscience) was reconstituted in ddH_20 at a concentration of 1.5 mM and stored at −20°C.

Venom gland transcriptomics

An adult *C. atrox* was collected in Portal, AZ under collecting permit 0456, and maintained in the UNC Animal Facility. Four days following manual venom extraction, the *C. atrox* was humanely euthanized and venom glands removed (IACUC protocol no. 9204). Approximately 70 mg of tissue, originating from both left and right venom glands, was homologized. Total RNA was isolated from homologized venom gland tissue using the previously described TRIzol (Life Technologies, C.A. U.S.A.) protocol for venom glands (77,78) A NEBNext Poly(A) mRNA Magnetic Isolation Module (New England Biolabs, MA, U.S.A) was used to select mRNA from 1 µg of total RNA, and the NEBNext Ultra RNA library prep kit (New England Biolabs, MA, U.S.A) manufacture's protocol followed to prepare the sample for Illumina® RNA-sequencing (RNA-seq). During library preparation, products within the 200-400 bp size range were selected by solid phase reversible immobilization with the Agencourt AMPure XP reagent (Beckman Coulter, C.A., U.S.A.) and PCR amplification consisted of 12 cycles. Final quantification of the RNA-seq library was done with the Library Quantification Kit for Illumina® platforms (KAPA Biosystems, M.A, U.S.A.). The *C. atrox* venom gland RNA-seq library was then checked for proper fragment size selection and quality on an Agilent 2100 Bioanalyzer, equally pooled with eight other unique barcoded RNA-seq libraries and sequenced on $1/8^{th}$ of an Illumina® HiSeq 2000 platform lane at the UC Denver Genomics core to obtain 125 bp paired-end reads.

To produce a comprehensive venom gland transcriptome database for *C. atrox,* two RNA-seq libraires were *de novo* assembled, the first from the *C. atrox* RNA-seq library detailed above and the second from a Texas locality *C. atrox* with reads available on the National Center for Biotechnology Information server (SRR3478367). Low quality reads were trimmed and adaptors removed using Trimmomatic (79) with a sliding window of 4 nucleotides and a

threshold of phred 30. Reads were then assessed with FastQC (Babraham Institute Bioinformatics, U.K.) to confirm that all adapters and low-quality reads were removed before *de novo* assembly. Three *de novo* assemblers were used in combination to produce a final, high-quality assembly: i). first, a Trinity (release v2014-07-17) genome-guided assembly was completed using default parameters and Bowtie2 (v2.2.6) (80) aligned reads to the *C. atrox* genome (provided by Noah Dowell (81)), ii) a second *de novo* assembly was completed with the program Extender (k-mer size 100) (82), performed with the same parameters as used for other snake venom glands (83), and with merged paired-end reads, merged with PEAR (Paired-End read mergeR v0.9.6; default parameters) (84), as seed and extension inputs, iii) a third *de novo* assembly was completed with VT Builder using default settings (85). From a concatenated fasta file of all three assemblies, coding contigs were then identified with EvidentialGene (downloaded May 2018) (86) and redundant coding contigs and those less than 150 bps were removed with CD-HIT (87,88). Reads were aligned with Bowtie2 to coding contigs and abundances determined with RSEM (RNA-seq by Expectation-Maximization; v1.2.23) (89). Contigs less than 1 TPM (Transcript Per Million) were filtered out, and the remaining contigs annotated with Diamond (90) BLASTx (E-value 10^{-05} cut-off) searches against the NCBI non-redundant protein database. Transcripts were identified as venom proteins after each was manually examined to determine if the resulting protein was full-length, shared sequence identity to a currently known venom protein, and contained a shared signal peptide sequence with other venom proteins within that superfamily. This transcript set was also filtered through ToxCodAn (91) as a final toxin annotation check, and the resulting translated toxins used as a custom database for mass spectrometry.

Venom Meltome Generation

Thermal profiling assays were carried out following previously described methods (74,92). Venom (1 µg/µL) was assayed in duplicate and divided into 10 aliquots of 20 µL and transferred to 0.2 mL PCR tubes. Each aliquot was individually heated at a fixed temperature over the range of 37° to 75°C for 3 min in a Bioer LifeECO™ thermal cycler (Figure 1a). Samples were allowed to aggregate at room temperature for one minute and then placed on ice. Precipitated proteins were removed by centrifugation at 21,000 x g for 45 min and the supernatant was removed and subjected to sodium dodecyl sulfate polyacrylamide gel electrophoresis (SDS-PAGE) and sample preparation for mass spectrometric analysis.

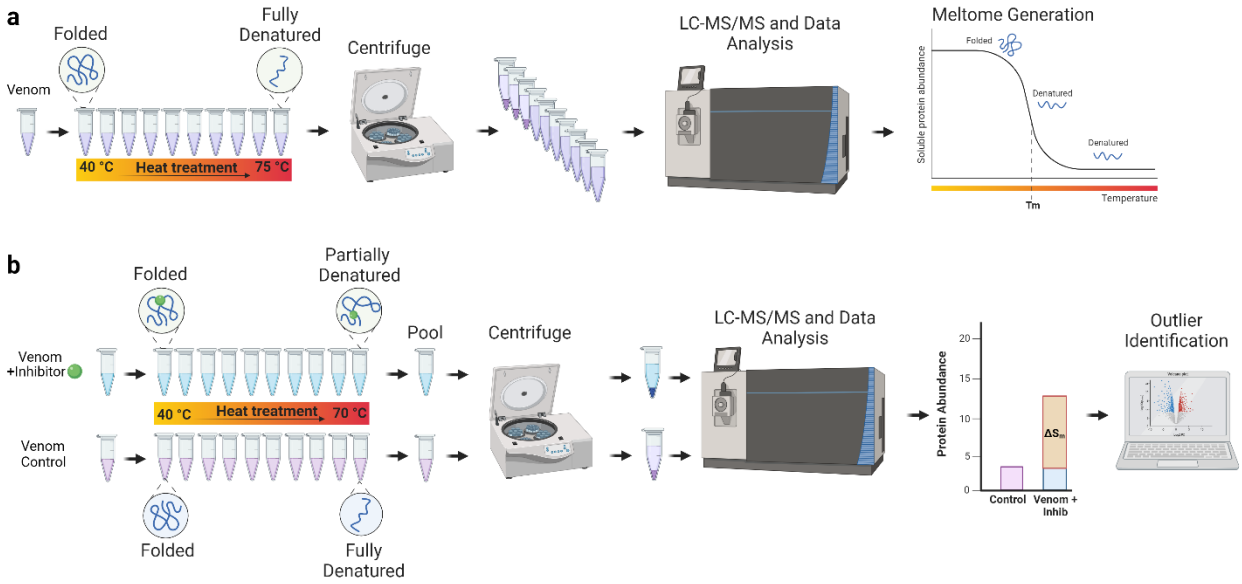

Figure 1. TPP (a) and PISA (b) workflows. a) In TPP experiments, samples are heated between 40 – 70°C and centrifuged to pellet denatured proteins. Samples are reduced, alkylated, and trypsin digested and analyzed with LC-MS/MS for protein identification. Melting curves are generated in ProSAP using unique intensity for each protein identified. T_m = melting temperature of 50% of population. b) In PISA, venom is incubated for 30 minutes at 37°C with an inhibitor or alone. Samples are heated from 40-70°C, and pooled before centrifuging to pellet insoluble material. Samples are prepared as mentioned above and analyzed via LC-MS/MS for protein identification. To identify inhibitor targets, unique intensity is used to calculate SAR values for each protein followed by identification of significant outliers.

244 *Inhibitor PISA Assays*

245 Venom (1 µg/µL) was incubated with two previously explored concentrations of
246 marimastat, 15 µM or 150 µM (53,61), or a vehicle control (ddH_2O) for 30 min at 37°C. Each
247 sample was then divided into 12 aliquots of 20 µL in 0.2 mL PCR tubes. Each aliquot was
248 individually heated at a different temperature from 40 to 70°C for 3 min in a Bioer LifeECO™
249 Thermal cycler (Figure 1b), allowed to cool at room temperature for one min, and placed on ice.
250 An equal volume of sample from each temperature point was pooled and centrifuged at 21,000 x
251 g for 45 min at 4°C to separate the soluble fraction from insoluble denatured proteins (70).
252 Because of the previously characterized differences in performance between supernatant and
253 pellet, we investigated both fractions (75,76). Approximately 30 µg of soluble protein (based on
254 control samples) was collected and prepared for mass spectrometry and 20 µg was used for gel
255 electrophoresis. PISA assays for each condition were performed in triplicate. Because selection
256 of a narrower temperature window for heat denaturation has been shown to increase sensitivity
257 of the PISA assay (73), we also performed a temperature gradient denaturation with 5
258 temperatures (selected based on SVMP family-level T_m values) from 56 to 60°C. Samples were
259 pooled and processed as described above.

260 *High-Performance Liquid Chromatography (HPLC)*

261 One mg of venom incubated with either 150 µM marimastat or a vehicle control (ddH_2O)
262 was subjected to reverse phase HPLC after heat treatment using a Waters system, Empower
263 software, and a Phenomenex Jupiter C_{18} (250 × 4.6 mm, 5 µm, 300 Å pore size) column as
264 outlined in Smith and Mackessy (93). Proteins/peptides were detected at 280 nm and 220 nm
265 with a Waters 2487 Dual λ Absorbance Detector. Fractions corresponding to each peak were
266 then frozen at -80ºC overnight, lyophilized, and then separated with SDS-PAGE as previously

267 described (93). Percent peak area and peak height at 280 nm were recorded as a proxy for
268 relative toxin abundance.

269 *Sodium dodecyl sulfate polyacrylamide gel electrophoresis (SDS-PAGE)*

270 SDS-PAGE materials were obtained from Life Technologies, Inc. (Grand Island, NY,
271 USA). Dithiothreitol (DTT)-reduced venom (20 µg) or lyophilized protein (approximately 5 µg –
272 reverse-phase high-performance liquid chromatography (RP-HPLC) fractionated) was loaded
273 into wells of a NuPAGE Novex Bis-Tris 12% acrylamide Mini Gel and electrophoresed in MES
274 buffer under reducing conditions for 45 min at 175 V; 7 µL of Mark 12 standards were loaded
275 for molecular weight estimates. Gels were stained overnight with gentle shaking in 0.1%
276 Coomassie brilliant blue R-250 in 50% methanol and 20% acetic acid (v/v) and destained in 30%
277 methanol, 7% glacial acetic acid (v/v) in water until background was sufficiently destained
278 (approximately 2 hours). Gels were then placed in storage solution (7% acetic acid, v/v) for
279 several hours with gentle shaking at room temperature and imaged on an HP Scanjet 4570c
280 scanner.

281 *Sample preparation for Liquid chromatography-tandem mass spectrometry (LC-MS/MS)*

282 The volume of supernatant corresponding to 30 µg of unmelted (soluble) protein was
283 dried in a speed vacuum and redissolved in 8 M urea/0.1 M Tris (pH 8.5) and reduced with 5
284 mM TCEP (tris (2-carboxyethyl) phosphine) for 20 min at room temperature. Samples were then
285 alkylated with 50 mM 2-chloroacetamide for 15 min in the dark at room temperature, diluted 4-
286 fold with 100 mM Tris-HCl (pH 8.5), and trypsin digested at an enzyme/substrate ratio of 1:20
287 overnight at 37°C. To stop the reaction, samples were acidified with formic acid (FA), and
288 digested peptides were purified with Pierce™ C18 Spin Tips (Thermo Scientific #84850)

289 according to the manufacturer's protocol. Samples were dried in a speed vacuum and redissolved
290 in 0.1% FA.

291 Electrophoretic protein bands subjected to LC-MS/MS were excised from Coomassie-
292 stained gels, destained, and subjected to in-gel reduction, alkylation, and overnight trypsin
293 digestion as previously described (94). Following the overnight digestion, samples were acidified
294 with 5% formic acid (FA) and tryptic peptides were extracted in 30 µl of 50% acetonitrile /1%
295 FA. Digests were dried in a vacuum centrifuge and redissolved in 0.1% FA for mass
296 spectrometry.

297 *Nano liquid chromatography tandem mass spectrometry*

298 Nano Liquid Chromatography tandem mass spectrometry (Nano-LC-MS/MS) was
299 performed using an Easy nLC 1000 instrument coupled with a Q-Exactive™ HF Mass
300 Spectrometer (both from ThermoFisher Scientific). Approximately 3 µg of digested peptides
301 were loaded on a C_{18} column (100 µm inner diameter × 20 cm) packed in-house with 2.7 µm
302 Cortecs C_{18} resin, and separated at a flow rate of 0.4 µL/min with solution A (0.1% FA) and
303 solution B (0.1% FA in ACN) under the following conditions: isocratic at 4% B for 3 min,
304 followed by 4%-32% B for 102 min, 32%-55% B for 5 min, 55%-95% B for 1 min and isocratic
305 at 95% B for 9 min. Mass spectrometry was performed in data-dependent acquisition (DDA)
306 mode. Full MS scans were obtained from *m/z* 300 to 1800 at a resolution of 60,000, an automatic
307 gain control (AGC) target of 1×10^6, and a maximum injection time (IT) of 50 ms. The top 15
308 most abundant ions with an intensity threshold of 9.1×10^3 were selected for MS/MS acquisition
309 at a 15,000 resolution, 1×10^5 AGC, and a maximal IT of 110 ms. The isolation window was set

to 2.0 *m/z* and ions were fragmented at a normalized collision energy of 30. Dynamic exclusion was set to 20 s.

Analysis of mass spectrometry data

Fragmentation spectra were interpreted against a custom protein sequence database generated from the assembly of *C. atrox* venom gland transcriptome data (described above) that was combined with UniProt entries of all toxins found in the *C. atrox* venom proteome reported by Calvete et al. (95) using MSFragger within the FragPipe computational platform (96,97). Reverse decoys and contaminants were included in the search database. Cysteine carbamidomethylation was selected as a fixed modification, oxidation of methionine was selected as a variable modification, and precursor-ion mass tolerance and fragment-ion mass tolerance were set at 20 ppm and 0.4 Da, respectively. Fully tryptic peptides with a maximum of 2 missed tryptic cleavages were allowed and the protein-level false discovery rate (FDR) was set to < 1%. The relative abundance of major snake venom toxin families was compared across samples using sum-normalized total spectral intensity (98).

Analysis of TPP data

Protein melting curves were generated by fitting sigmoidal curves to relative protein abundances using the Protein Stability Analysis Pod (ProSAP) package (99). The temperature at which relative protein abundance reached 50%, T_m (melting temperature), was determined in ProSAP by normalizing intensity to the lowest temperature (37°C), followed by normalization to the most thermostable proteins as previously described (76). Duplicates were averaged to determine the average T_m of all identified venom toxins. Venom proteins failing to reach 50% denaturation even at higher temperatures were classified as non-melting proteins.

Analysis of PISA data

PISA data was analyzed as previously described (71,98). Briefly, PISA uses the ΔS_m value or soluble abundance ratio (SAR) as opposed to the T_m to determine differences in thermal stability (70). ΔS_m represents the difference in integral abundance of a protein in treated compared to untreated samples. We performed a two-tailed Student's *t*-test with unequal variance to calculate p-values ($p<0.05$). Changes to venom protein abundance were visualized using volcano plots based on $\log_2$SAR values and $-\log_{10}$ transformed p-values. Proteins with a $\log_2$SAR value ≥ 0.5 and a $-\log_{10}$ transformed p-value ≥ 1.3 ($p<0.05$) were identified as toxins with a significant shift to thermal stability. All figures were made with BioRender.com.

Results

Crotalus atrox venom proteome

Previous characterization of the *C. atrox* venom proteome revealed the presence of at least 24 proteins belonging to eight different venom toxin protein families (Figure 2a; (95)) and, more recently, the presence of 31 SVMP genes in *C. atrox* with 15 to 16 expressed SVMPs (100). SVMPs and snake venom serine proteases (SVSPs) were the two most abundant protein families representing nearly 70% of the venom proteome. L-amino acid oxidase (L-AAO), Phospholipase A_2 (PLA_2), disintegrins, and cysteine-rich secretory proteins (CRISPs) comprise most of the remaining 25% of *C. atrox* venom proteins, whereas vasoactive peptides, endogenous SVMP inhibitors, and C-type lectins (CTL) comprised the remaining small fraction

of venom components comprising <2% of the venom proteome. Utilizing the protein databased generated using sequences of proteins identified by Calvete et al. (95) combined with protein sequences derived from a *C. atrox* venom gland transcriptome, we detected 46 unique proteoforms with at least one unique peptide in *C. atrox* venom (Figure 2b). Venom toxins with the highest number of distinct proteoforms detected included 13 CTLs, 13 SVMPs, nine SVSPs, and three PLA_2s (Figure 2b). We identified only one unique proteoform of more abundant proteins including L-AAO and CRISP and only one proteoform for minor components bradykinin-potentiating peptide (BPP), glutaminyl-peptide cyclotransferase (GPC), hyaluronidase (HYAL), nerve growth factor (NGF), phospholipase B (PLB), and vascular endothelial growth factor (VEGF).

RP-HPLC analysis revealed a complex toxin profile of *C. atrox* venom similar to that of Calvete et al., 2009 (Figure 2c). We used SDS-PAGE of peak fractions (Supplemental Figure 1) combined with the peak elution times and identified masses in Calvete et al. (95) to confirm peak identities. BPP's eluted between 8 and 15 min with co-elution of disintegrins and SVMP inhibitors. PLA_2 eluted at 27, 30, and between 39-44 min, CRISP eluted at 29 min, SVSP eluted between 32 – 36 min, and L-AAO eluted at 46 min. SVMPs eluted between 51-56 min (Figure 2c).

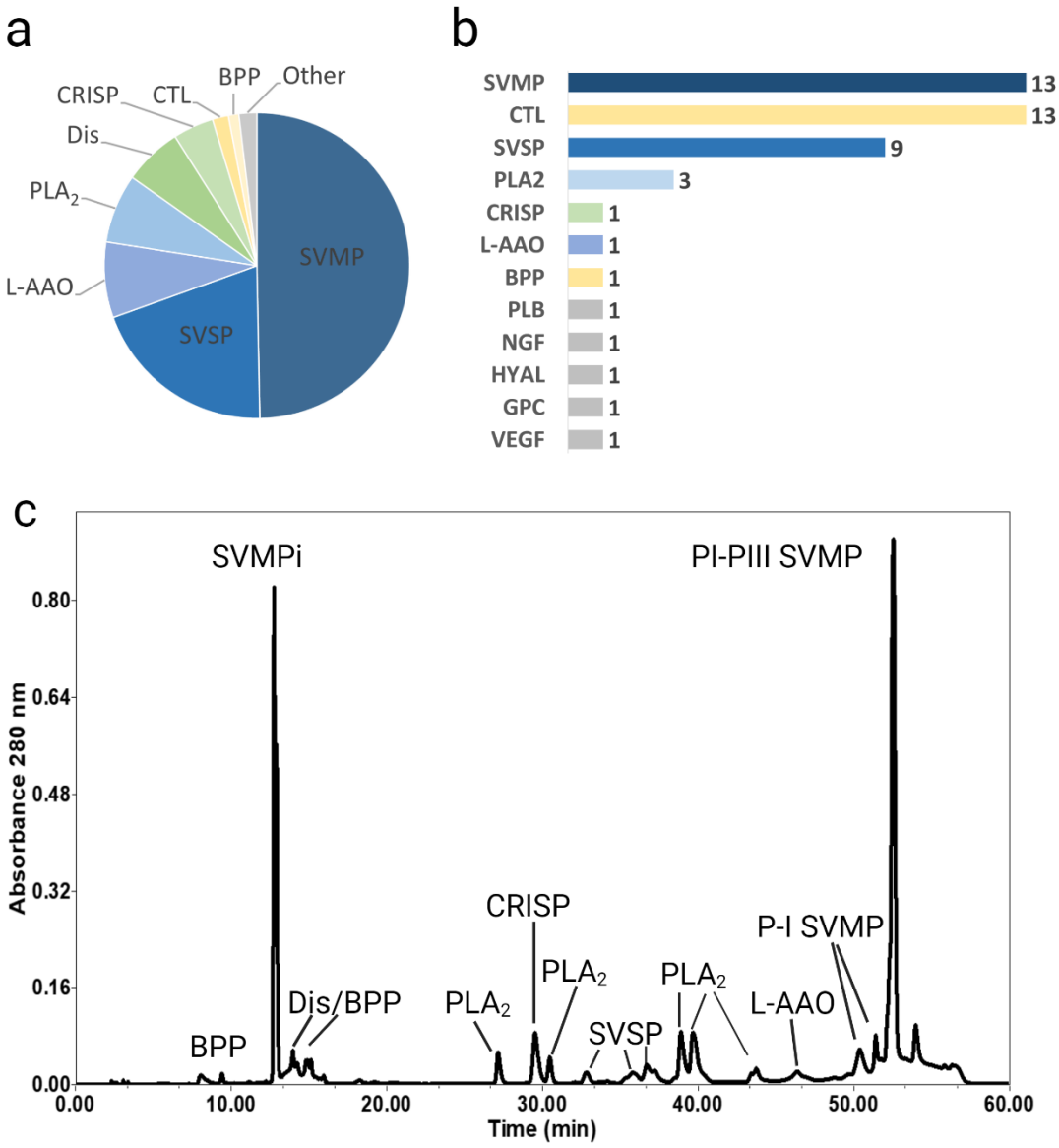

Figure 2. *Crotalus atrox* venom proteome characterization. a) Toxin family abundances in *C. atrox* venom modified from Calvete et al., 2009. b) The number of proteoforms identified in *C. atrox* venom in the present study organized by family. c) RP-HPLC separated *C. atrox* venom. For peak identification fractions were analyzed with mass spectrometry and SDS-PAGE and compared to known masses from Calvete et al., 2009. SVMP=Snake venom metalloprotease, CTL=C-type lectin, SVSP=snake venom serine protease, Dis=disintegrin, PLA_2 =phospholipase A_2, BPP=Bradykinin potentiating peptide, CRISP=cysteine rich secretory protein, L-AAO=L-amino acid oxidase, SVMPi= SVMP tripeptide inhibitor, PLB= Phospholipase B, NGF=nerve growth factor, HYAL=hyaluronidase, GPC=glutaminyl-peptide cyclotransferase, VEGF=vascular endothelial growth factor.

384 *C. atrox venom meltome*

385 With the goal of demonstrating the utility of applying a TPP workflow for identifying
386 venom protein interactions with a small molecule inhibitor, we first assessed the effects of
387 thermal stress on the venom proteome. Venom was subjected to increasing temperatures ranging
388 from 40 to 75°C, allowed to cool at room temperature, followed by separation and removal of
389 aggregates from each temperature point by centrifugation. The soluble fractions were then
390 visualized by gel electrophoresis (Figure 3a) and prepared for LC-MS/MS. SDS-PAGE analyses
391 of these fractions indicate that the entire venom proteome appeared to exhibit some degree of
392 denaturation between the temperatures tested with clear differences in denaturation observed
393 across venom protein families (Figure 3a). For example, L-AAO, HYAL, SVMPs, and CTLs
394 appeared more thermally sensitive while SVSP, CRISP, PLA_2, and disintegrin families exhibited
395 greater stability at higher temperatures.

396

397

398

399

400

401

402

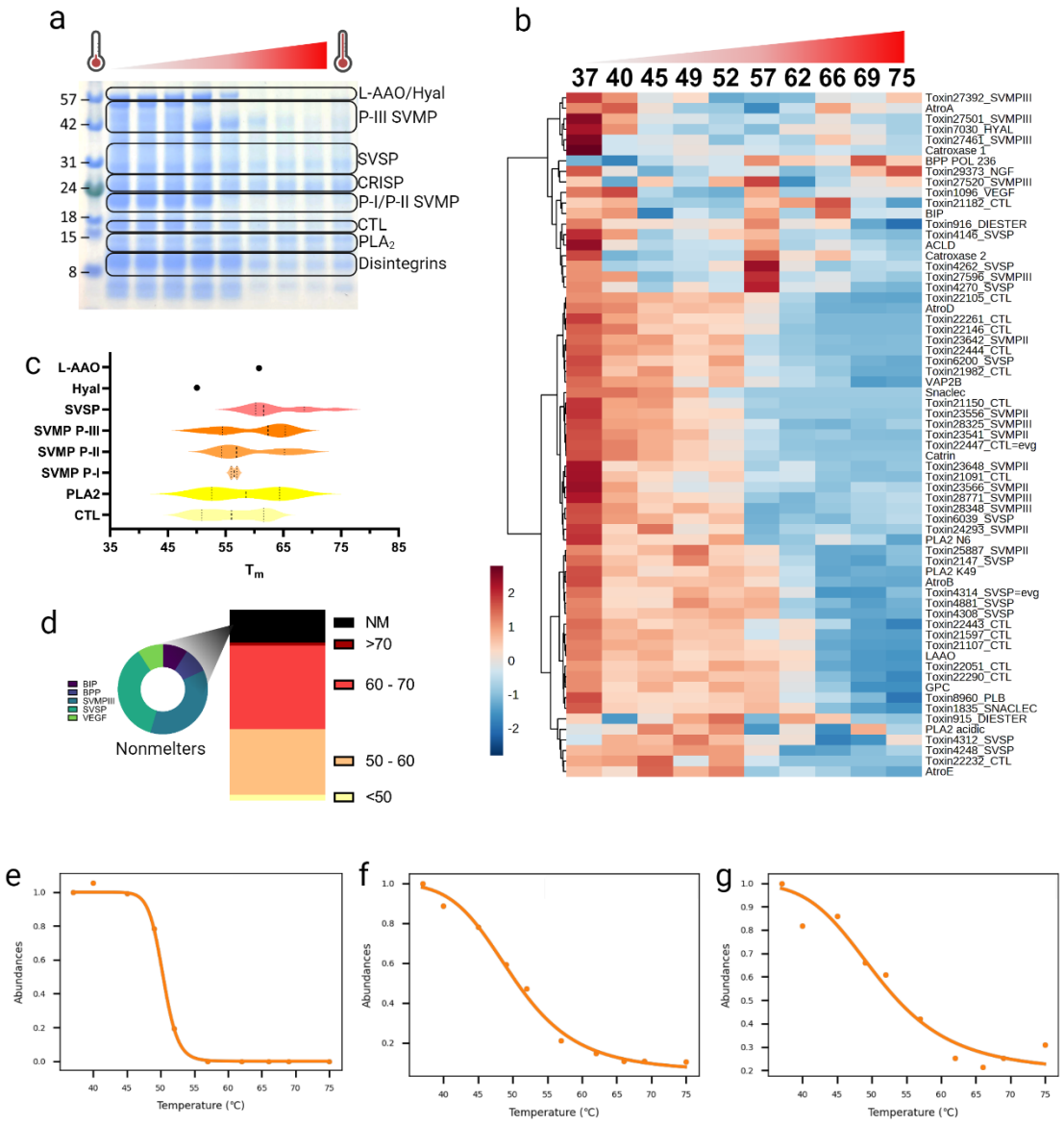

Figure 3. *C. atrox* meltome characterization. a) SDS-PAGE of *C. atrox* venom heated at temperatures between 37-70°C for 3 minutes. b) Heatmap showing the thermal denaturation of most toxin proteoforms across 10 temperatures where 37°C represents the nondenatured control. Heatmap colors represent normalized intensity and are scaled by row to better visualize variation in intensity between temperatures. c) Distribution of melting temperatures organized by family. Dotted lines represent median and quartile ranges. d) Distribution of melting temperatures for all toxins identified. Nonmelters (NM) are classified as proteoforms for which T_m could not be calculated when heated to a maximum temperature of 75°C. e) Representative melting curve of a CTL (Crotocetin). Abundance is normalized to 37°C f) Representative melting curve of a PLA_2 (Cvv-N6). Abundance is normalized to 37°C. g) Representative melting curve of an SVMP (PIII 28325). Abundance is normalized to 37°C.

Next, we assessed the thermal stability of venom proteins across the 10 different temperature points by LC-MS/MS. An equal volume of each soluble fraction was collected and subjected to reduction, alkylation, trypsin digestion, and LC-MS/MS. Fragmentation spectra were interpreted against our *C. atrox*-specific custom venom proteome sequence database, and we used the ProSAP package (99) to determine melting points for each venom protein family. When normalized to thermostable proteins, most venom proteins show decreasing abundance with increasing temperature, with the majority of proteins reduced in abundance at temperatures above 62°C (Figure 3b). The distribution of toxin melting temperature (T_m) values ranged from 47.8-74.3°C (Figure 3c and 3d). Most toxins had T_m's between 50-60°C (Fig 3d; n=22) or 60-70°C (n=28), and only 11 proteoforms were still thermostable with no calculable T_m at 75°C (BIP, BPP, VEGF, 4 SVMPIII, and 4 SVSPs; Fig 3d). The five toxins with the lowest T_m's included four CTLs (average T_m =49.3°C, stdev=1.1°C; Figure 3c and 3e) and the single hyaluronidase proteoform (T_m =50.6°C). CTLs T_m values as a whole ranged from 47.8-63.1°C (ave= 56.0°C, stdev=5.3°C). PLA_2s had an average T_m of 61.2°C (stdev=8.3°C; Figure 3c and 3f). The different SVMP subfamilies differed slightly in their melting range but were not significantly different (p=0.77; Figure 3c). PI-SVMP proteoforms had an average T_m of 56.8°C (stdev=0.03°C), PIIs averaged 59.3°C (stdev=5.7°C; Figure 3c), and PIII's averaged 59.7°C (stdev=6°C; Figure 3g). SVSPs had the highest average T_m (63.9°C, stdev=5.5°C), and made up a large proportion of the proteins that were thermostable above 75°C (Figure 3b). The single L-AAO proteoform identified melted at 61.7°C. In general, melting temperatures were reproducible between replicates with an average standard deviation of 1.17°C between replicates. These results demonstrate protein family-level differences in thermal stability, in that all proteoforms of some families denatured (i.e., CTL, SVMP I) when subjected to heat, while others appear

437 resistant to thermal perturbation (SVSPs). These results indicate that a significant proportion of
438 the venom proteome is amenable to thermal denaturation.

439 *Venom-wide interactions with marimastat*

440 After establishing that venom proteins are susceptible to thermal denaturation, we next
441 assessed if a TPP strategy could be applied to elucidate small molecule-venom protein
442 engagement. For this, we applied the PISA assay, a simplified TPP approach where samples
443 across the entire temperature gradient of the same treatment are pooled prior to preparation and
444 mass spectrometric analysis (66,70,71). With traditional PISA, the abundance of the protein(s) in
445 the soluble fractions of the pooled samples is then used to assess the effect of a compound on its
446 thermal stability (70). For highly thermostable proteins, monitoring supernatant alone is likely
447 not effective in thermal-shift-based methods (76). Because binding of a compound can, in some
448 cases, lead to protein destabilization rather than stabilization, quantifying protein abundance in
449 the precipitate pellet can also identify protein targets (76). Further, because of different observed
450 signal-to-noise ratios, soluble and pelleted material may perform differently in PISA assays to
451 identify significant thermal shifts (75,76). Utilizing precipitated material to measure changes in
452 protein stability can additionally reduce the false discovery rate (FDR) and improve sensitivity of
453 the assay. Based on this logic, we utilized both supernatant and precipitated material to
454 investigate the effects of marimastat.

455 PISA assays were performed on marimastat, an inhibitor of matrix metalloproteases that
456 has shown significant inhibitory activity against SVMPs (50,51,53,56,60–62). *Crotalus atrox*
457 venom was incubated with marimastat (15 μM and 150 μM) or vehicle (ddH_2O) for 30 min at
458 37°C. Following incubation, each sample was divided into 12 aliquots and subjected to

increasing temperatures from 40 to 70°C. Equal aliquots per temperature point were then pooled, protein aggregates were separated by centrifugation, and the soluble and insoluble fractions of the vehicle and inhibitor-treated venoms were prepared for downstream analysis.

When filtering criteria were applied ($p<0.05$, and $log_2SAR >0.5$), the lower concentration of marimastat (15 µM) caused five of 21 SVMP proteoforms supernatant (PIII 28348, PIII 28325, PII 25887, PII 23541, and VAP 1) to display a stabilizing shift in treated supernatant compared to untreated supernatant (Figure 4a). In addition to these five proteoforms, two additional SVMPs (PII 23556 and PII 27392) were more abundant in the supernatant of venom treated with 150 µM of marimastat (Figure 4b).

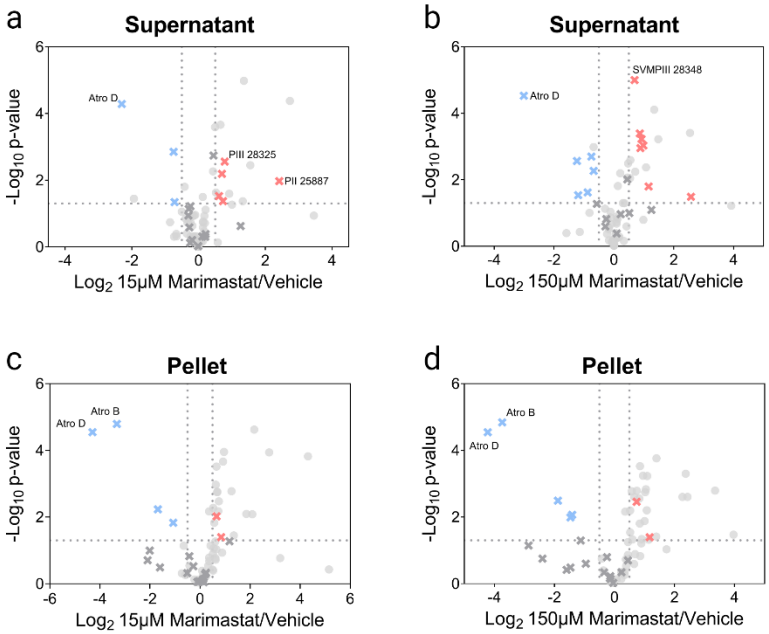

Figure 4. *C. atrox* venom-wide interactions with two concentrations of marimastat with temperature window from 40-70°C. a) Volcano plot comparing soluble supernatant of heat-treated venom + marimastat (15 µM) to heat-treated venom alone. X indicates SVMP proteoforms, red=positive outliers, blue=negative outliers, grey=not significant. b) Volcano plot comparing soluble supernatant of heat-treated venom + marimastat (150 µM) to heat-treated venom alone. c) Volcano plot comparing insoluble precipitate of heat-treated venom + marimastat (15 µM) to heat-treated venom alone. d) Volcano plot comparing insoluble precipitate of heat-treated venom + marimastat (150 µM) to heat-treated venom alone.

Next, we compared the pellets of untreated venom to venom treated with both concentrations of marimastat. When filtering criteria were applied at the low concentration, only four SVMPs (Atro B, Atro-D, SVMPIII 27520, and SVMPIII 28348) were detected at significantly lower abundance in the treated pellet compared to the control pellet, indicative of a stabilizing effect of marimastat (Figure 4c). These same proteoforms, in addition to SVMP PII 23541, were also significantly reduced in the pellet of the higher marimastat concentration (Figure 4d). The presence of positive outliers identified in both the supernatant and negative outliers in the precipitate of treated venom indicates an overall stabilizing effect of marimastat on venom targets.

Validation of inhibitor interactions

To validate our PISA results showing the stabilizing effects of marimastat on SVMPs, we performed SDS-PAGE and RP-HPLC on non-heat-denatured venom and venoms treated with marimastat or vehicle. The toxin family composition of the peaks and bands altered by the addition of marimastat was confirmed by mass spectrometry (Supplemental Tables 1-2). In the heated marimastat-treated venom, gel bands A and B were composed predominantly of PIII 27501 and VAP2B (band A) and PII 23556, Atro E and Atro B (band B; Figure 5a). Band C was composed of acidic PLA_2, band D of PLA2 Cax-K49, CTL 22443, and PLA2 Cvv-N6, and band E was predominantly CTL 21182, CTL 22444, and PLA2 Cax-K49. SDS-PAGE analysis of the heat-denatured and undenatured control venom shows a clear reduction in the size and intensity of SVMP-PIII (~50kDa; band A), SVMP P-I/II (~20kDa; band B), and CTL/PLA_2 gel bands (~10-14kDa; bands C-E) in response to thermal treatment (Figure 5a). This reduction in SVMP and CTL/PLA_2 band size and intensity in response to heat appears to be partially to fully recovered when venom is incubated with 150 μM marimastat (Fig. 5a).

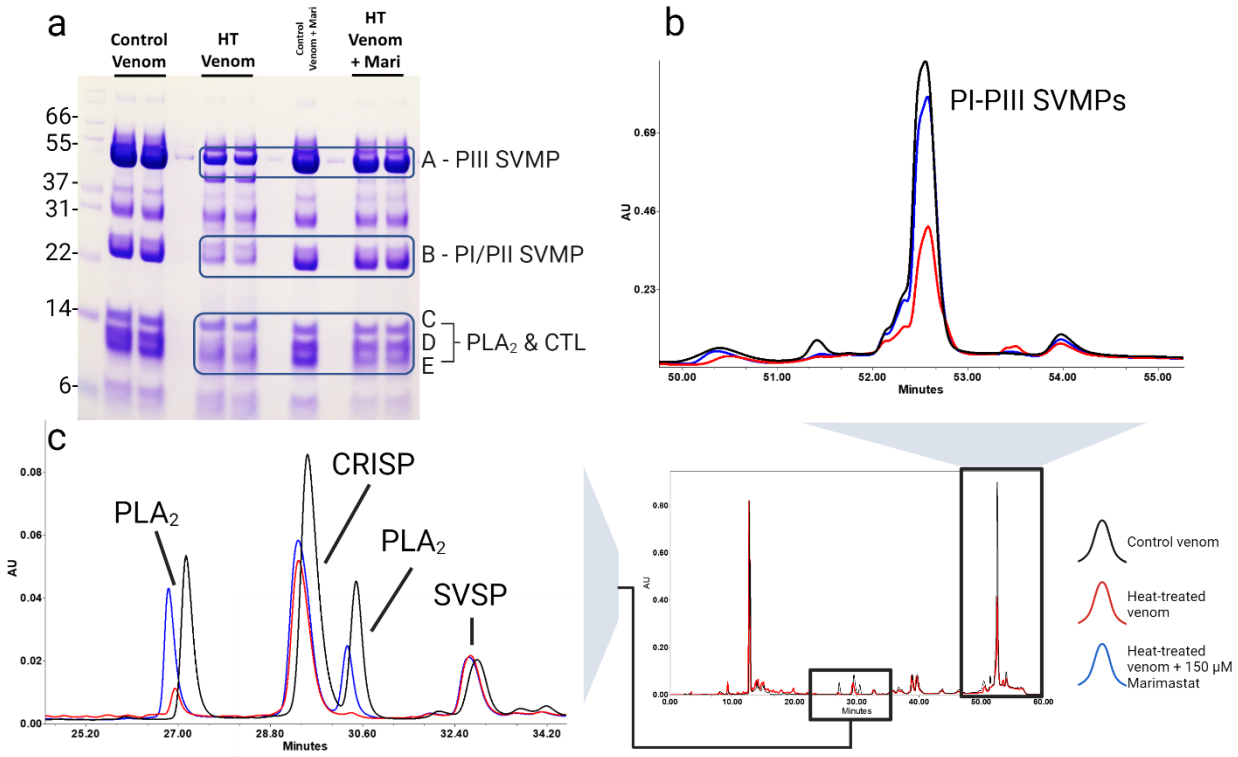

Figure 5. Validation assays of inhibitor interactions. a) SDS-PAGE comparison of heat-treated venom to heat-treated venoms incubated with 150 µM of marimastat with a thermal window of 40-70°C. Note the recovery in band size and intensity of SVMP and PLA_2 bands in marimastat-treated samples. Left side indicates molecular mass standards in kDa. b) Enlarged HPLC-separated SVMP peak overlay comparing abundance of non-heat-treated venom (black), heat-treated venom (red), and venom heat-treated after incubation with 150 µM of marimastat (blue). Note the recovery of peak area in the inhibitor-treated sample. c) Enlarged HPLC-separated PLA_2 peak overlay comparing abundance of non-heat-treated venom (black), heat-treated venom (red), and venom heat-treated after incubation with 150 µM of marimastat (blue). Note the recovery of PLA_2 peak area in the inhibitor-treated sample.

RP-HPLC peaks eluting between 51 to 54 minutes were identified by mass spectrometry as SVMPs, with VAP2B, PIII 27501, P-III ACLD, PII 23556, PIII 28348, PII 23566, and Atro E representing the dominant proteoforms. These continued to be the dominant proteoforms with the exception of Atro E in both the heated control and marimastat-treated venoms. The 27-minute, 29-minute, and 30-minute peaks were composed predominantly of the basic PLA_2 Cax-

515 K49, CRISP, and basic PLA_2 Cvv-N6 respectively (Figure 5c). These remained the dominant
516 proteoforms in the heated control venom and marimastat-treated venom, with the exception of
517 marimastat-treated peak 30 where CRISP became the dominant proteoform followed by PLA_2
518 Cvv-N6.

519 The stabilizing effect of marimastat on some venom proteins is further demonstrated by
520 analysis of RP-HPLC, which shows partial recovery in the chromatographic peak area and peak
521 height of SVMP and two PLA_2 peaks in the marimastat-treated venoms compared to the controls
522 (Fig 5b-c). After heat treatment, SVMPs lose 44% of their original peak area, but marimastat
523 treatment results in only a 7% decrease in peak area after melting (Figure 5b). The PLA_2 proteins
524 eluting at 27 minutes decreases by 75% when venom is heat-treated and only 26% when venom
525 is treated with marimastat, while the PLA_2 eluting at 30 minutes is virtually absent in the heated
526 control venom but only loses 52% abundance when heat-treated with marimastat (Figure 5c).
527 Peak heights of PLA_2 (27 minutes), PLA_2 (30 minutes), and SVMPs decrease by 81%, 100%, and
528 57% respectively after melting; however, with marimastat peak height only decreases by 21%,
529 48%, and 21% respectively (Figure 5b-c).

530 VAP2B is the dominant proteoform in *C. atrox* venom (Figure 5b; Supplemental Table 2)
531 and was the second most abundant proteoform in the SVMP fractions and gel bands of treated
532 venom. However, it was not detected as a stabilized outlier in either supernatant or pellet in the
533 current PISA experiments performed with the temperate range of 40 to 70°C. Thus, we aimed to
534 increase the sensitivity of the PISA assay with a narrower thermal window determined by the T_m
535 values previously calculated for the target toxin family.

536

Venom-wide interactions with marimastat in a narrowed thermal window PISA

While PISA is advantageous because it reduces the analysis time and sample preparation while still being effective at target discovery, it may sacrifice sensitivity compared to TPP experiments due to the pooling of all temperature points, and melting temperature selection can have a drastic effect on thermal behavior in PISA experiments (73,76). To investigate this, we compared the performance of a broad thermal window (40-70°C) to a narrower window (56-60°C), selected based on the mean and standard deviation of T_m's of the target venom toxin family. We performed PISA assays with the same concentrations of marimastat, with a narrower temperature window from 56-60°C with 5 temperature points of each sample replicate, which has been shown to improve the overall sensitivity of the PISA assay in target identification (73).

When samples were heat treated with a narrower window of temperatures, the lower concentration of marimastat displayed three of 21 SVMP proteoforms (PIII 28348, PIII 28325, PII 23541) at a greater abundance in treated supernatant compared to untreated supernatant (Figure 6a). At the higher concentration, seven of 21 proteoforms were higher in supernatant of treated venom: VAP1, PIII 28348, PIII 28325, PII 23556, PII 23541, PIII 28771, PIII 27392 (Figure 6b). In the pellets of samples treated with a narrower range of temperatures, 11 of 21 proteoforms (VAP2B, PIII 28348, Atro D, PIII 27501, PII 23541, Atro B, PIII 27461, PIII 27520, PIII 28771, PII 23648, PIII 27392) demonstrated a stabilizing shift in the pellet of the lower concentration of marimastat condition (Figure 6c). These same proteoforms plus PII 23556 were reduced in the pellet at the higher concentration of marimastat (Figure 6d).

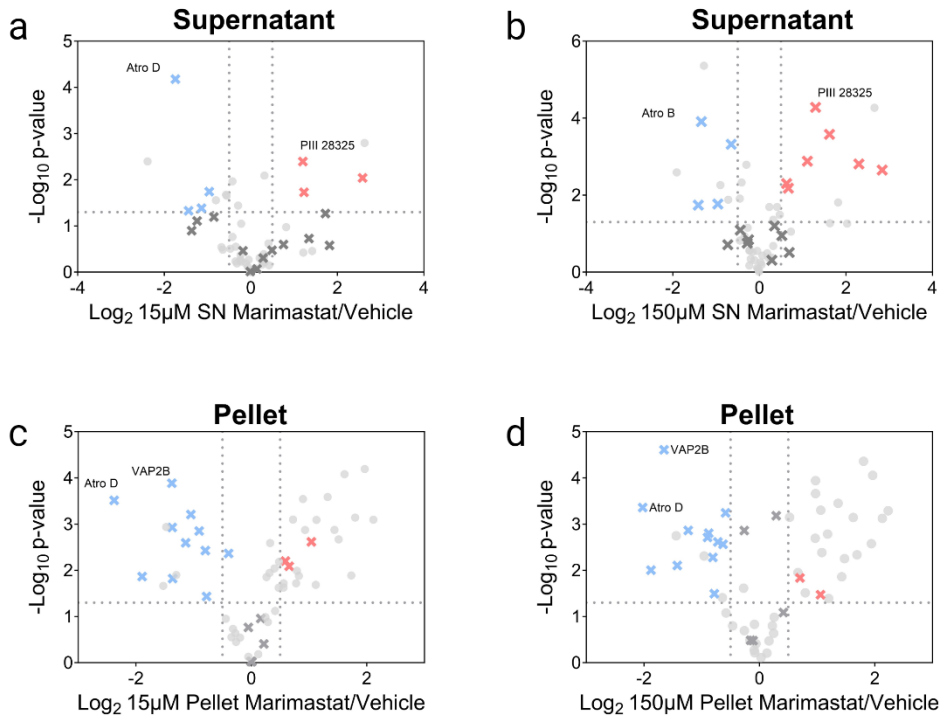

Figure 6. *C. atrox* venom-wide interactions with two concentrations of marimastat with temperature window from 56-60°C. a) Volcano plot comparing soluble supernatant of heat-treated venom + marimastat (15 μM) to heat-treated venom alone. X indicates SVMP proteoforms, red=positive outliers, blue=negative outliers, grey=not significant. b) Volcano plot comparing soluble supernatant of heat-treated venom + marimastat (150 μM) to heat-treated venom alone. c) Volcano plot comparing insoluble precipitate of heat-treated venom + marimastat (15 μM) to heat-treated venom alone. d) Volcano plot comparing insoluble precipitate of heat-treated venom + marimastat (150 μM) to heat-treated venom alone.

Heat-treatment comparison

Next, we compared the performance of a broad thermal window (40-70°C) and narrower thermal window (56-60°C) to our results gathered from our validation experiments (Figures 4-6). At both temperature ranges when venom was treated with marimastat, principal component analysis (PCA) shows clustering of the replicates based on treatment condition, with the two marimastat-treated groups separating from the vehicle-treated samples (Figure 7a-d). These results indicate that both concentrations of marimastat interact with venom protein targets and

alter the thermal stability of venom proteins compared to the control group. However, pellet replicates (Figures 7c-d) cluster more tightly together in both conditions than in supernatants with greater separation among the treatment groups (Figures 7a-b). The highest amount of variance explained (97%) by the top two principal components was in the narrow window pellet, though all plots had a high percentage of sample variance explained (>86%). The number of significantly stabilized proteins found in the supernatant ($p<0.05$, $\log_2 SAR >0.5$) after treatment with marimastat at a broad melting window were 12 and 14 for 15 μM and 150 μM, respectively (Figure 7e). The percentage of SVMPs among the identified proteins were 42% and 50%. At the narrower melting window, four and nine proteins were identified in 15 μM and 150 μM treatments, respectively, but SVMPs comprised 75% and 78% of identified proteins. In general, pellets of both melting windows appeared to perform better regardless of concentration. The precipitated pellet from 150 μM-treated venom heated at the narrower thermal window identified the most SVMP proteoforms of any treatment group. Though the broader temperature window precipitate identified fewer SVMP proteoforms, SVMPs were the only venom toxin family proteoforms identified, while the supernatant appeared to contain more, potentially off-target, non-SVMP identifications. The broad melting window identified four and five SVMP proteoforms, while the narrow window pellets identified 11 and 12 for 15 μM and 150 μM, respectively (Figure 7e).

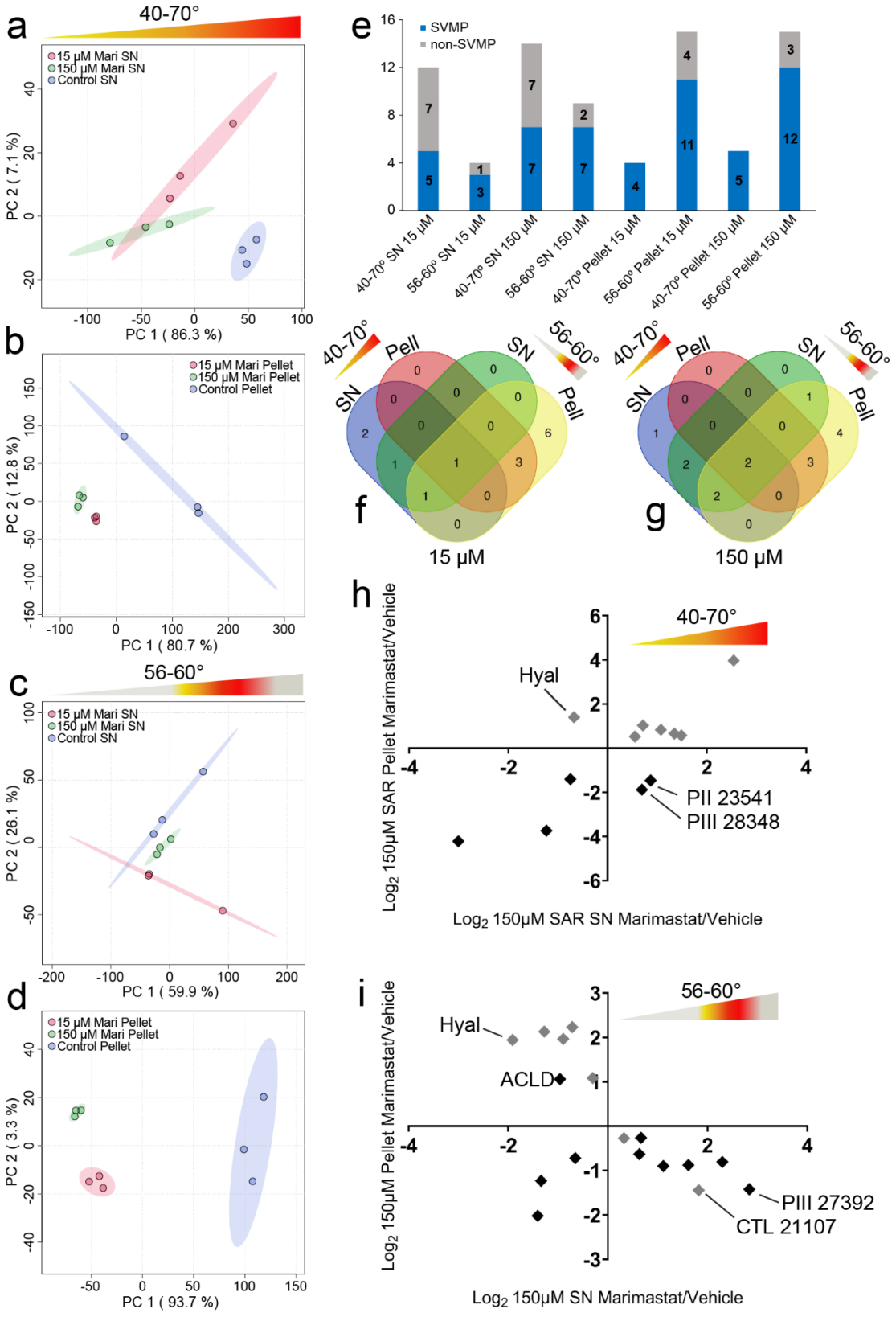

Figure 7. Comparison of a broad (40-70°C) to a narrow (56-60°C) PISA thermal window. PCA plot comparing replicates of soluble supernatant of a) heat-treated venom + 15 μM marimastat to heat-treated venom alone and b) heat-treated venom + 150 μM marimastat to heat-treated venom alone. SN= supernatant, Pell= pellet, Con= control. PCA plot with 95% confidence intervals comparing replicates of insoluble precipitate of c) heat-treated venom + 15 μM marimastat to heat-treated venom alone and d) heat-treated venom + 150 μM marimastat to heat-treated venom alone. SN= supernatant, Pell=pellet. SN= supernatant, Pell= pellet, Con= control. e) Number of SVMP and non-SVMP proteins identified with significant thermal shifts toward stabilization (p-value<0.05 log_2SAR>0.5) after 15 μM or 150 μM marimastat treatment in supernatants and pellets heat-treated at a broad (40-70°C) or a narrow (56-60°C) thermal window. SN=supernatant, P=pellet. Venn diagrams of SVMP proteins identified with significant thermal shifts toward stabilization (p-value<0.05, log_2SAR>0.5) in supernatants and pellets heat-treated at a broad (40-70°C) or a narrow (56-60°C) thermal window after f) 15 μM or g) 150 μM marimastat treatment. SN= supernatant, Pell=pellet. Scatter plot showing log_2SAR values calculated from 150 μM marimastat-treated venom vs. vehicle treatment heated at from h) 40-70°C or i) 56-60°C that meet significance criteria in both supernatant (SN) and precipitate (Pellet) group. Largest outliers of SVMP and non-SVMP proteoforms are labeled. SN=supernatant. Black=SVMP proteoforms, grey=non-SVMP toxins. SN= supernatant, Hyal=hyaluronidase, ACLD=PIII SVMP ACLD, CTL= C-type lectin.

Performance of specific SVMP proteoform identification between melting windows varied significantly at both concentrations, with only one common proteoform at 15 μM (Figure 7f) and two at 150 μM (Figure 7g). At both concentrations, the narrow window pellets had the highest number of uniquely identified SVMP proteoforms. When soluble abundance ratios (log_2SAR) of supernatant and pellets are compared, the narrower thermal window performs significantly better at identifying target and off-target proteoforms that meet significance criteria in both supernatant and pellet. When only proteins meeting significance criteria for both supernatant and pellet were compared, the broad window performed poorly, identifying only two SVMPs (PIII 28348, PII 23541). with significant stabilizing shifts (Figure 7h). The narrower window identified six SVMP proteoforms with significant stabilizing shifts (VAP1, PII 23556, PIII 28348, PIII 28771, PII 23541, PIII 27392) and one with a possible destabilizing shift (ACLD; Figure 7i). Off-target proteins that met significance criteria for both conditions included hyaluronidase, and, using the narrower window, three SVSPs and VEGF.

SVMP comparisons and target identification

Because the narrower temperature window appears to identify more target proteoforms with less noise, we utilized this narrow window approach to re-analyze interactions between SVMPs and marimastat. More SVMP proteoforms were identified as significant with a narrower window when analyses of the supernatant and pellet are combined (Figure 7e-g), and analyses of the pellet identified more SVMP proteoforms than the supernatant within the narrower thermal window (Figure 8a). Specifically, analysis of the narrow range pellet identified highly abundant proteins also identified in the validation assays but not identified using the broad the broad thermal window (e.g., VAP2B). Hierarchical clustering analysis comparing supernatants and pellets at both concentrations shows an inverse relationship between relative intensity of each proteoform in the pellet vs. the supernatant (Figure 8b). When these conditions are compared to controls, we resolved three patterns of various proteoforms: 1) proteoforms that showed a positive shift (trend towards stabilization) in the supernatant at both concentrations of marimastat; 2) proteoforms that disappear from the pellet after marimastat treatment but do not necessarily increase in SAR in the supernatant (trend towards stabilization); and 3) proteoforms that increase in pellet SAR after treatment (Figure 8c). Finally, correlation analysis performed with the SAR values of proteoforms supernatants and pellets of the narrow thermal window identified three clusters of proteoforms with similar shifts in thermal behavior: 1) a cluster containing the proteoforms that were stabilized by marimastat (e.g., VAP2B, 27501, 23556, 27392) that represent the strongest targets of marimastat, 2) a cluster containing atrolysin B, atrolysin D, and PIII 27520 which appeared to decrease in abundance in both supernatants and pellets after marimastat treatment, and 3) a cluster that did not appear to be thermally stabilized by marimastat including atrolysin A, PII 24293 (Figure 8d). The strongest target list includes

652 proteoforms identified in the validation protein gel (e.g., VAP2B, PIII 27501, PII 23556, PIII
653 28348, PIII 27392, and PII 23648), and those identified as most abundant in the SVMP HPLC
654 peaks (VAP2B, PIII 27501, PII 23556, PIII 28348, PIII 27461).

655 The most abundant proteoforms were identified as significant in analysis of the pellet but
656 not in the corresponding supernatant. To further explore the apparently superior performance of
657 analysis of the pellet for identifying high abundance targets, we use VAP2B as an example. In
658 the case of VAP2B, the stabilizing effect of marimastat is only evident in the pellet, and both 15
659 μM and 150 μM concentrations have significantly lower levels of the precipitated toxin
660 ($p=0.003$, $p=0.0013$, respectively, Figure 8e). A less abundant proteoform, PIII 28348, had a
661 stabilizing shift that was detected in both the pellet and the supernatant at both concentrations of
662 marimastat (Figure 8f). In the pellet, abundance of PIII 28348 was significantly lower at both
663 concentrations than in the untreated control ($p=0.0004$, $p=0.0014$, respectively), and significantly
664 higher in the supernatant compared to control ($p<0.0001$).

665

666

667

668

669

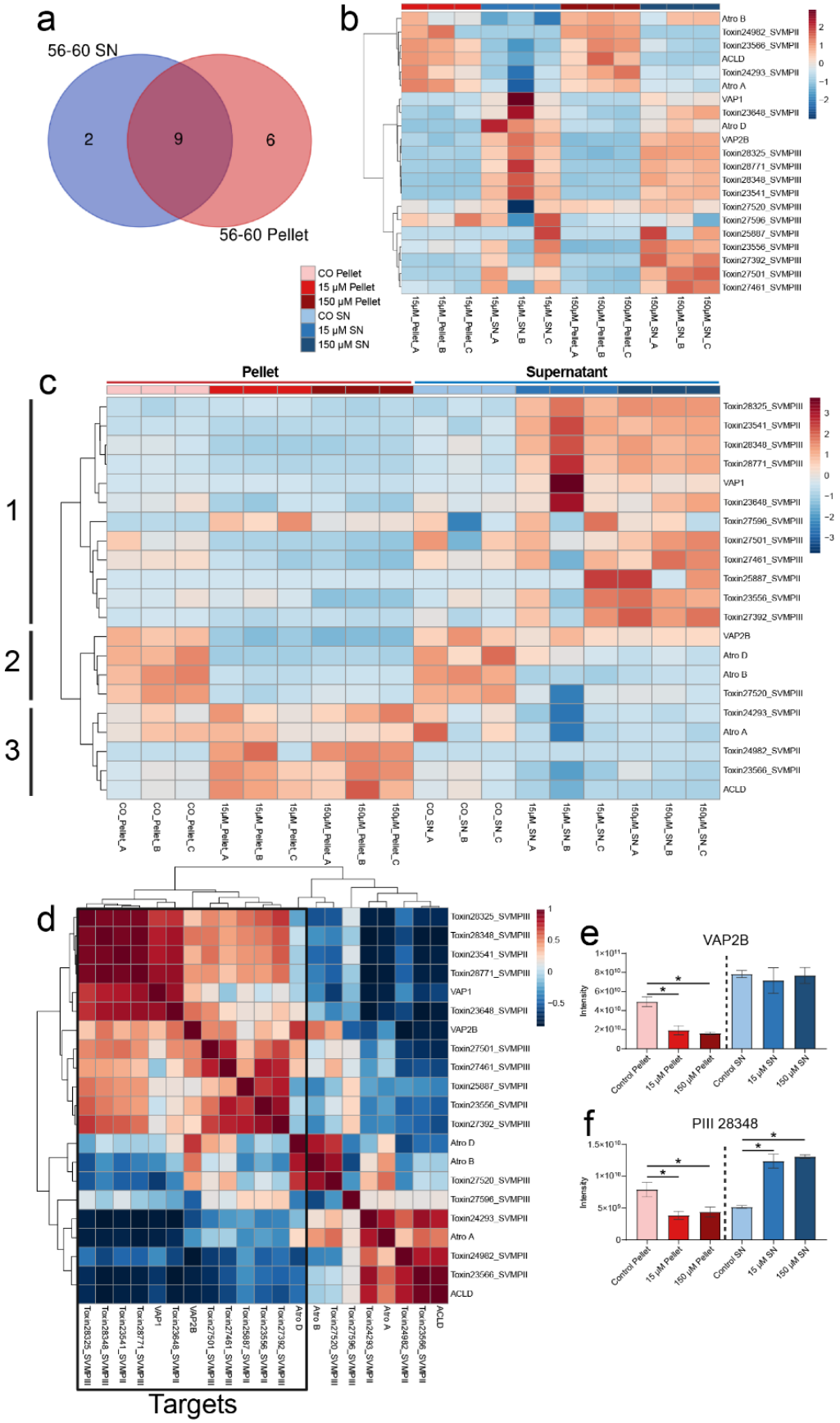

Figure 8. Effects of marimastat treatment and a narrow thermal window on SVMP proteoforms only. a) Number of proteins identified in supernatant (SN) and pellet of narrow thermal window that meet significance criteria (p-value<0.01, log_2SAR>0.5) b) heatmap of sum-normalized intensity values in supernatant or precipitate of SVMPs from 15 μM or 150 μM marimastat treated venom. Heatmap colors are scaled by row to better visualize variation in sum-normalized intensity between classes. c) heatmap of sum-normalized intensity values in supernatant or precipitate of SVMPs from 15 μM or 150 μM marimastat treated venom or vehicle control showing concentration-dependent shifts in abundance. Heatmap colors are scaled by row to better visualize variation in sum-normalized intensity between classes. d) Correlation plot of SAR values showing strongest marimastat targets based on effects of marimastat treatment on SVMP proteoform intensity. Comparison of concentration-dependent intensity shifts between precipitate and supernatant of e) the most abundant SVMP proteoform VAP2B and f) a less abundant SVMP proteoform PIII 28348 at both concentrations of marimastat at the narrow thermal window.

Off-target effects

Based on recovery of peak area in PLA_2 and CTL-containing peaks and gel bands in marimastat-treated venom subjected to RP-HPLC (Figure 5c), we explored the possibility of using PISA assays to detect off-target effects of marimastat. Interestingly, at both concentrations with the wider thermal window we observed changes in thermal behavior indicative of a shift towards stabilization of some non-target protein families, including two PLA_2 proteoforms (Cax-K49 and Cvv-N6) and four CTL proteoforms. In the gels, there was recovery of band E containing Cax-K49, and CTL's 22443, 21182, and 22444. Both PLA_2 proteoforms were repeated positive outliers in supernatants of all conditions but were not significant in any pellets. Various CTL proteoforms including CTL 21107, 22105, 22447, 21150, and 22232 were significant outliers in some conditions. When comparing only significant log_2SAR values in both supernatant and pellet, hyaluronidase, VEGF, 2 SVSPs and 2 CTL's (22444, 21107) were significantly correlated between pellet and supernatant at the narrower melt window, but only hyaluronidase displayed stabilizing behavior (Figure 7i).

Discussion

The development and testing of alternative snakebite therapeutics that are affordable, stable, and easily administered is an urgent global need (1,10,47,101). Small molecule inhibitors currently lead the field of possible supplementary snake envenomation therapies, with phase II clinical trials ongoing for the PLA_2 inhibitor varespladib (102) and the SVMP inhibitor DMPS ((103); Clinical Trials.gov, 2021). Numerous inhibitors have shown promising cross-species efficacy *in vivo* and *in vitro* (37,50,53,57,104), indicating that they may be less vulnerable to the effects of venom variation than traditional antibody-based antivenoms. However, additional preclinical studies are needed to evaluate the neutralizing efficacy and specificity of these drugs alone and in combination, and the development of these drugs would be accelerated by implementation of high throughput screening of interactions and efficacy across many species. Research on small molecule inhibitors of snake venom toxins has typically focused on *in vitro* and *in vivo* functional assays based on the known or likely biological activities of toxins (49,50,108,51–53,58,104–107). These approaches utilize a downstream measurement of the presumed interactions of an inhibitor with its targets (ex. reduced specific activity or increased survival). A previous study performed molecular docking analysis using marimastat and a purified PI SVMP proteoform CAMP-2 to demonstrate a direct interaction (51). However, the PISA method outlined here represents both a direct and venom-wide assessment of target-ligand engagement and provides the opportunity to link direct target-ligand interactions with functional and phenotypic responses (71,72,109).

In this study, we investigate the thermal characteristics of the *C. atrox* venom proteome and use this to develop a PISA-based assessment of the venom proteome-wide targets of the SVMP inhibitor marimastat. We investigate both its proteome-wide effects and determine and

723 validate its interactions with specific venom proteoforms of its target toxin family (SVMPs) as
724 well as possible off-target protein families. We identified a suite of marimastat proteoform-level
725 targets and confirmed them by RP-HPLC and SDS-PAGE**.** We also compared the performance
726 of soluble supernatant and insoluble precipitate at two different inhibitor concentrations for
727 target identification. Our results provide a promising first assessment of the application of a
728 PISA-based approach as a sensitive and high-throughput method to assess the direct targets of
729 small molecule inhibitors for snake venom. Based on our experiments with PISA in this context,
730 we find that analysis of the insoluble fraction from venom that was treated with a high
731 concentration of marimastat, but a narrow thermal window for PISA, provided more sensitive
732 target data with the least noise.

733 Previous research has shown that small molecule inhibitor efficacy *in vitro* may not
734 always translate to *in vivo* efficacy. For example, the SVMP inhibitors dimercaprol and
735 prinomastat showed moderate to high SVMP inhibitory activity *in vitro* but failed to confer any
736 protection towards crude venom in *in vivo* assays (60). Furthermore, studies have highlighted
737 cross-species variation in neutralization effects of potential inhibitors, which has significant
738 implications for the application of inhibitors as broadly effective pre-hospital treatments of
739 envenomation by potentially diverse species (58). Dimercaprol showed promise in murine
740 models as an SVMP inhibitor against *Echis ocellatus* venom (110), however, it lacked this
741 protective effect *in vivo* against *Dispholidus typus* venom (60), likely due to the high levels of
742 divergence in venom composition between these distantly related species. While some inhibitors
743 have demonstrated neutralization capacity of specific biological effects (such as anticoagulation)
744 caused by venoms of divergent species, they may vary in effectiveness across species because of
745 lineage-specific variation in venom toxin sequence, activity, or relative abundance or because the

same biological effects may arise due to the action of different toxin families altogether (58,60). Knowledge of the snake species-specific venom-wide and proteoform-specific efficacy of inhibitors has the potential to significantly improve our ability to predict cross-species neutralization and to unravel the disparity between *in vitro* and *in vivo* results.

Before PISA could be widely applied for the screening of a large number of potential inhibitors against snake venom, a number of considerations must be addressed. By pooling a wide range of temperature points, PISA data in particular may suffer from reduced screening sensitivity, depending on the specific thermal properties of various proteins (73). Venom toxins appears to have significantly higher T_m values than human cell types, which ranged from 48 to 52°C (92). Some potential snake venom toxin families of interest (i.e., SVSPs and CRISPs) display high thermal tolerance, which generally suggests that a thermal shift assay would be less than ideal to investigate inhibitor-toxin interactions for such thermostable proteoforms. Based on the target family-level thermal properties determined by TPP, we refined our PISA assay parameters to a more sensitive thermal window for target identification and showed that a narrower thermal window selection can improve inhibitor target identification. These findings highlight how knowledge of general thermal properties of a toxin family of interest might be used to improve target identification, perhaps even for protein families with higher thermal stability.

Our results demonstrate how analysis of the composition of both supernatants and pellets can be complementary, and thus be integrated to further refine inferences of molecular targets (75,76). In our experiments, we observed varying performances between supernatant and pellet data in the consistent identification of inhibitor targets, particularly of the high abundance SVMP proteoform VAP2B. We found that precipitated material of the narrowed thermal window

769 provided enhanced sensitivity for target deconvolution of the most abundant toxins and across
770 the proteome in general. As previously noted, precipitated material produces better signal-to-
771 noise ratios and more apparent stability ratios compared to analysis of supernatant (75). Indeed,
772 some previously investigated well-known drug targets were only identified in the precipitated
773 material, with no corresponding stability ratio shift in the supernatant (75), as seen with VAP2B
774 in our study, indicating that pelleted material is not just complementary to supernatant-based
775 results, but may be critical for thorough target deconvolution. This is likely due to the continued
776 presence of many proteins even at high temperatures as observed in this study and in previous
777 studies (75). We also note a concentration-dependent effect of marimastat on target
778 identification, where the higher concentration provided both a higher number of targets and less
779 noise compared to the lower concentration of marimastat.

780 In addition to providing information about direct target interactions, PISA also allows for
781 off-target effects to be investigated. Off-target binding of a drug may result in adverse effects
782 that decrease (or complicate) its therapeutic utility (109,111), and small molecule drugs in
783 particular tend to bind a myriad of molecular targets (112). For example, inhibitors of serine
784 proteases exist that may be effective against medically significant snake venom serine proteases
785 (SVSPs), but they may also cross-react with endogenous serine proteases in human plasma,
786 which are critical for normal coagulation cascade activation (58). Our PISA analyses identified
787 evidence of the interaction of marimastat with off-target toxin families, including CTLs and
788 PLA_2 toxins, which were also supported by our liquid chromatography and gel electrophoresis
789 results. These findings are also consistent with prior studies that have shown marimastat and
790 another SVMP inhibitor, prinomastat, can reduce PLA_2-based anticoagulant venom effects (54).
791 While CTLs are a minor and less clinically relevant component of *C. atrox* venom (95), PLA_2s

792 are more likely to be medically significant and tend to be fairly ubiquitous and abundant across
793 diverse snake venoms (24,113–115). Though we did not detect any reduction in PLA_2 activity in
794 marimastat-treated samples (data not shown), off-target effects should be considered when
795 investigating small molecule inhibitors of snake venom toxins, as they may demonstrate effects
796 on other medically significant targets and/or contribute to unexpected outcomes *in vivo*.

797 Multiple snake venom gene families have undergone substantial gene family expansion,
798 diversification, and neofunctionalization that has in many cases resulted in elevated rates of
799 nonsynonymous substitutions in regions of these proteins that determine biological function (12).
800 This trend has been observed in SVMPs (116), SVSPs (117), PLA_2s (118,119), and 3FTXs
801 (120), and has resulted in large multi-gene toxin families with similar structure but a wide array
802 of biological functions and pharmacological effects which can also vary substantially across
803 species (5,9,11,13,121). Indeed, this diversity of proteoforms within and across species presents
804 an extreme challenge for the development of effective therapeutics to target the effects of these
805 diverse and species-specific toxin cocktails. A major step to addressing this challenge has
806 resulted in efforts to identify the most bioactive and medically relevant toxic proteins and
807 proteoforms in venom using "omics" technologies, which has been referred to as
808 "toxicovenomics" (122–125). A PISA-based approach in combination with toxicovenomics has
809 the potential to take the key next step to address this complex problem through the screening of
810 molecules that may neutralize the action of venom toxins across a wide variety of species that
811 display high variability of medically significant venom toxin families, proteoforms, and
812 activities. PISA and other high-throughput approaches provide promising paths forward for
813 screening of large numbers of commonly studied and currently unexplored inhibitors against a
814 wide scope of venoms for more rapid development of alternative snakebite therapies.

Literature Cited

1. Gutiérrez JM, Calvete JJ, Habib AG, Harrison RA, Williams DJ, Warrell DA. Snakebite envenoming. Nat Rev Dis Prim. 2017 Sep 14;3(1):17063.

2. Chippaux JP. Snakebite envenomation turns again into a neglected tropical disease! J Venom Anim Toxins Incl Trop Dis. 2017 Aug 8;23(1):1–2.

3. Minghui R, Malecela MN, Cooke E, Abela-Ridder B. WHO's Snakebite Envenoming Strategy for prevention and control. Vol. 7, The Lancet Global Health. 2019.

4. Casewell NR, Wagstaff SC, Harrison RA, Renjifo C, Wüster W. Domain loss facilitates accelerated evolution and neofunctionalization of duplicate snake venom metalloproteinase toxin genes. Mol Biol Evol. 2011;28(9):2637–49.

5. Casewell NR. Evolution: Gene Co-option Underpins Venom Protein Evolution. Curr Biol. 2017;27(13):R647–9.

6. Hargreaves AD, Swain MT, Hegarty MJ, Logan DW, Mulley JF. Restriction and recruitment-gene duplication and the origin and evolution of snake venom toxins. Genome Biol Evol. 2014;6(8):2088–95.

7. Casewell NR, Wüster W, Vonk FJ, Harrison RA, Fry BG. Complex cocktails: The evolutionary novelty of venoms. Trends Ecol Evol. 2013;28(4):219–29.

8. Vonk FJ, Casewell NR, Henkel C V., Heimberg AM, Jansen HJ, McCleary RJR, et al. The king cobra genome reveals dynamic gene evolution and adaptation in the snake venom system. Proc Natl Acad Sci U S A. 2013;110(51):20651–6.

9. Casewell NR, Huttley GA, Wüster W. Dynamic evolution of venom proteins in squamate reptiles. Nat Commun. 2012;3.

10. Williams DJ, Gutiérrez JM, Calvete JJ, Wüster W, Ratanabanangkoon K, Paiva O, et al. Ending the drought: New strategies for improving the flow of affordable, effective antivenoms in Asia and Africa. J Proteomics. 2011;74(9):1735–67.

11. Casewell NR, Wagstaff SC, Wuster W, Cook DAN, Bolton FMS, King SI, et al. Medically important differences in snake venom composition are dictated by distinct postgenomic mechanisms. Proc Natl Acad Sci U S A. 2014;111(25):9205–10.

12. Sunagar K, Jackson TNW, Undheim EAB, Ali SA, Antunes A, Fry BG. Three-fingered RAVERs: Rapid Accumulation of Variations in Exposed Residues of snake venom toxins. Toxins (Basel). 2013;5(11).

13. Brust A, Sunagar K, Undheim EAB, Vetter I, Yang DC, Casewell NR, et al. Differential evolution and neofunctionalization of snake venom metalloprotease domains. Mol Cell Proteomics. 2013 Mar 1;12(3):651–63.

14. Olaoba OT, Karina dos Santos P, Selistre-de-Araujo HS, Ferreira de Souza DH. Snake Venom Metalloproteinases (SVMPs): A structure-function update. Toxicon X. 2020;7.

15. Castro AC, Escalante T, Rucavado A, Gutiérrez JM. Basement membrane degradation and inflammation play a role in the pulmonary hemorrhage induced by a P-III snake venom metalloproteinase. Toxicon. 2021 Jul 15;197:12–23.

16. Gutiérrez JM, Rucavado A. Snake venom metalloproteinases: Their role in the

855 pathogenesis of local tissue damage. Biochimie. 2000;82(9–10):841–50.

856 17. Terra RMS, Pinto AFM, Guimarães JA, Fox JW. Proteomic profiling of snake venom
857 metalloproteinases (SVMPs): Insights into venom induced pathology. Toxicon.
858 2009;54(6):836–44.

859 18. Gutiérrez JM, Escalante T, Rucavado A, Herrera C. Hemorrhage caused by snake venom
860 metalloproteinases: A journey of discovery and understanding. Toxins (Basel). 2016 Mar
861 26;8(4).

862 19. Brown N, Landon J. Antivenom: The most cost-effective treatment in the world? Toxicon.
863 2010 Jun 15;55(7):1405–7.

864 20. Agarwal R, Aggarwal AN, Gupta D, Behera D, Jindal SK. Low dose of snake antivenom
865 is as effective as high dose in patients with severe neurotoxic snake envenoming. Emerg
866 Med J. 2005 Jun 1;22(6):397–9.

867 21. Jones BK, Saviola AJ, Reilly SB, Stubbs AL, Arida E, Iskandar DT, et al. Venom
868 Composition in a Phenotypically Variable Pit Viper (Trimeresurus insularis) across the
869 Lesser Sunda Archipelago. J Proteome Res. 2019;18(5).

870 22. Ciscotto PHC, Rates B, Silva DAF, Richardson M, Silva LP, Andrade H, et al. Venomic
871 analysis and evaluation of antivenom cross-reactivity of South American Micrurus
872 species. J Proteomics. 2011 Aug 24;74(9):1810–25.

873 23. Tanaka GD, Furtado MDFD, Portaro FCV, Sant'Anna OA, Tambourgi D V. Diversity of
874 Micrurus snake species related to their venom toxic effects and the prospective of

875 antivenom neutralization. PLoS Negl Trop Dis. 2010 Mar;4(3):e622.

876 24. Petras D, Sanz L, Segura Á, Herrera M, Villalta M, Solano D, et al. Snake venomics of
877 African spitting cobras: Toxin composition and assessment of congeneric cross-reactivity
878 of the Pan-African EchiTAb-Plus-ICP antivenom by antivenomics and neutralization
879 approaches. J Proteome Res. 2011 Mar 4;10(3):1266–80.

880 25. Casewell NR, Cook DAN, Wagstaff SC, Nasidi A, Durfa N, Wüster W, et al. Pre-clinical
881 assays predict Pan-African Echis viper efficacy for a species-specific antivenom. PLoS
882 Negl Trop Dis. 2010 Oct;4(10):e851.

883 26. Casewell NR, Jackson TNW, Laustsen AH, Sunagar K. Causes and Consequences of
884 Snake Venom Variation. Trends Pharmacol Sci. 2020;41(8):570–81.

885 27. Saviola AJ, Pla D, Sanz L, Castoe TA, Calvete JJ, Mackessy SP. Comparative venomics
886 of the Prairie Rattlesnake (*Crotalus viridis viridis*) from Colorado: Identification of a
887 novel pattern of ontogenetic changes in venom composition and assessment of the
888 immunoreactivity of the commercial antivenom CroFab®. J Proteomics. 2015;121:28–43.

889 28. Mackessy SP, Williams K, Ashton KG. Ontogenetic variation in venom composition and
890 diet of *Crotalus oreganus concolor*. A case of venom paedomorphosis? Copeia.
891 2003;(4):769–82.

892 29. Cipriani V, Debono J, Goldenberg J, Jackson TNW, Arbuckle K, Dobson J, et al.
893 Correlation between ontogenetic dietary shifts and venom variation in Australian brown
894 snakes (Pseudonaja). Comp Biochem Physiol Part - C Toxicol Pharmacol. 2017 Jul
895 1;197:53–60.

30. Modahl CM, Mukherjee AK, Mackessy SP. An analysis of venom ontogeny and prey-specific toxicity in the Monocled Cobra (*Naja kaouthia*). Toxicon. 2016;119:8–20.

31. Saviola AJ, Gandara AJ, Bryson RW, Mackessy SP. Venom phenotypes of the Rock Rattlesnake (Crotalus lepidus) and the Ridge-nosed Rattlesnake (Crotalus willardi) from México and the United States. Toxicon. 2017;138.

32. Smith CF, Nikolakis ZL, Ivey K, Perry BW, Schield DR, Balchan NR, et al. Snakes on a plain: biotic and abiotic factors determine venom compositional variation in a wide-ranging generalist rattlesnake. BMC Biol. 2023 Jun 6;21(1):136.

33. Senji Laxme RR, Attarde S, Khochare S, Suranse V, Martin G, Casewell NR, et al. Biogeographical venom variation in the indian spectacled cobra (Naja naja) underscores the pressing need for pan-india efficacious snakebite therapy. PLoS Negl Trop Dis. 2021 Feb 1;15(2):e0009150.

34. Chanda A, Patra A, Kalita B, Mukherjee AK. Proteomics analysis to compare the venom composition between Naja naja and Naja kaouthia from the same geographical location of eastern India: Correlation with pathophysiology of envenomation and immunological cross-reactivity towards commercial polyantiv. Expert Rev Proteomics. 2018;

35. Chanda A, Kalita B, Patra A, Senevirathne WDST, Mukherjee AK. Proteomic analysis and antivenomics study of Western India Naja naja venom: correlation between venom composition and clinical manifestations of cobra bite in this region. Expert Rev Proteomics. 2019;16(2):171–84.

36. Tan CH, Tan KY, Sim SM, Fung SY, Tan NH. Geographical venom variations of the

Southeast Asian monocled cobra (Naja kaouthia): Venom-induced neuromuscular depression and antivenom neutralization. Comp Biochem Physiol Part - C Toxicol Pharmacol. 2016 Jul 1;185–186:77–86.

37. Gutiérrez JM, Albulescu LO, Clare RH, Casewell NR, Abd El-Aziz TM, Escalante T, et al. The search for natural and synthetic inhibitors that would complement antivenoms as therapeutics for snakebite envenoming. Toxins (Basel). 2021 Jun 29;13(7):451.

38. Waiddyanatha S, Silva A, Siribaddana S, Isbister GK. Long-term Effects of Snake Envenoming. Toxins (Basel). 2019 Apr 1;11(4).

39. Williams SS, Wijesinghe CA, Jayamanne SF, Buckley NA, Dawson AH, Lalloo DG, et al. Delayed psychological morbidity associated with snakebite envenoming. PLoS Negl Trop Dis. 2011;5(8).

40. Rivel M, Solano D, Herrera M, Vargas M, Villalta M, Segura Á, et al. Pathogenesis of dermonecrosis induced by venom of the spitting cobra, Naja nigricollis: An experimental study in mice. Toxicon. 2016;119.

41. Gutiérrez JM, León G, Rojas G, Lomonte B, Rucavado A, Chaves F. Neutralization of local tissue damage induced by Bothrops asper (terciopelo) snake venom. In: Toxicon. 1998.

42. Gutiérrez JM. Improving antivenom availability and accessibility: Science, technology, and beyond. Toxicon. 2012;60(4).

43. Gutiérrez JM, Williams D, Fan HW, Warrell DA. Snakebite envenoming from a global

perspective: Towards an integrated approach. Toxicon. 2010 Dec;56(7):1223–35.

44. De Silva HA, Ryan NM, De Silva HJ. Adverse reactions to snake antivenom, and their prevention and treatment. Br J Clin Pharmacol. 2016;81(3).

45. Fan HW, Monteiro WM. History and perspectives on how to ensure antivenom accessibility in the most remote areas in Brazil. Toxicon. 2018;151.

46. Cristino JS, Salazar GM, Machado VA, Honorato E, Farias AS, Vissoci JRN, et al. A painful journey to antivenom: The therapeutic itinerary of snakebite patients in the Brazilian Amazon (the QUALISnake study). PLoS Negl Trop Dis. 2021;15(3).

47. Habibid AG, Musa BM, Iliyasuid G, Hamza M, Kuznik A, Chippauxid JP. Challenges and prospects of snake antivenom supply in Sub-Saharan Africa. PLoS Negl Trop Dis. 2020 Aug 1;14(8):1–10.

48. Chippaux JP. Estimate of the burden of snakebites in sub-Saharan Africa: A meta-analytic approach. Toxicon. 2011;57(4).

49. Xie C, Slagboom J, Albulescu LO, Somsen GW, Vonk FJ, Casewell NR, et al. Neutralising effects of small molecule toxin inhibitors on nanofractionated coagulopathic Crotalinae snake venoms. Acta Pharm Sin B. 2020 Oct 1;10(10):1835–45.

50. Albulescu L-O, Xie C, Ainsworth S, Alsolaiss J, Crittenden E, Dawson CA, et al. A therapeutic combination of two small molecule toxin inhibitors provides broad preclinical efficacy against viper snakebite. Nat Commun. 2020 Dec 15;11(1):6094.

51. Layfield HJ, Williams HF, Ravishankar D, Mehmi A, Sonavane M, Salim A, et al.

Repurposing Cancer Drugs Batimastat and Marimastat to Inhibit the Activity of a Group I Metalloprotease from the Venom of the Western Diamondback Rattlesnake, Crotalus atrox. Toxins (Basel). 2020 May 9;12(5):309.

52. Fontana Oliveira IC, Gutiérrez JM, Lewin MR, Oshima-Franco Y. Varespladib (LY315920) inhibits neuromuscular blockade induced by Oxyuranus scutellatus venom in a nerve-muscle preparation. Toxicon. 2020;187:101–4.

53. Arias AS, Rucavado A, Gutiérrez JM. Peptidomimetic hydroxamate metalloproteinase inhibitors abrogate local and systemic toxicity induced by Echis ocellatus (saw-scaled) snake venom. Toxicon. 2017;132:40–9.

54. Chowdhury A, Lewin MR, Zdenek CN, Carter R, Fry BG. The Relative Efficacy of Chemically Diverse Small-Molecule Enzyme-Inhibitors Against Anticoagulant Activities of African Spitting Cobra (Naja Species) Venoms. Front Immunol. 2021;12.

55. Clare RH, Hall SR, Patel RN, Casewell NR. Small Molecule Drug Discovery for Neglected Tropical Snakebite. Vol. 42, Trends in Pharmacological Sciences. 2021.

56. Hall SR, Rasmussen SA, Crittenden E, Dawson CA, Bartlett KE, Westhorpe AP, et al. Repurposed drugs and their combinations prevent morbidity-inducing dermonecrosis caused by diverse cytotoxic snake venoms. bioRxiv. 2022;1–40.

57. Gutiérrez JM, Lewin MR, Williams DJ, Lomonte B. Varespladib (LY315920) and methyl varespladib (LY333013) abrogate or delay lethality induced by presynaptically acting neurotoxic snake venoms. Toxins (Basel). 2020;12(2).

977 58. Youngman NJ, Lewin MR, Carter R, Naude A, Fry BG. Efficacy and Limitations of
978 Chemically Diverse Small-Molecule Enzyme-Inhibitors against the Synergistic
979 Coagulotoxic Activities of Bitis Viper Venoms. Molecules. 2022;27(5).

980 59. Lewin MR, María Gutiérrez J, Samuel SP, Herrera M, Bryan-Quirós W, Lomonte B, et al.
981 Delayed oral LY333013 rescues mice from highly neurotoxic, lethal doses of papuan
982 taipan (Oxyuranus scutellatus) venom. Toxins (Basel). 2018;10(10).

983 60. Menzies SK, Clare RH, Xie C, Westhorpe A, Hall SR, Edge RJ, et al. In vitro and in vivo
984 preclinical venom inhibition assays identify metalloproteinase inhibiting drugs as potential
985 future treatments for snakebite envenoming by Dispholidus typus. Toxicon X. 2022 Jun
986 1;14:100118.

987 61. Xie C, Albulescu L-O, Bittenbinder MA, Somsen GW, Vonk FJ, Casewell NR, et al.
988 Neutralizing Effects of Small Molecule Inhibitors and Metal Chelators on Coagulopathic
989 Viperinae Snake Venom Toxins. Biomedicines. 2020 Aug 20;8(9):297.

990 62. Bittenbinder MA, Bergkamp ND, Slagboom J, Bebelman JPM, Casewell NR, Siderius
991 MH, et al. Monitoring Snake Venom-Induced Extracellular Matrix Degradation and
992 Identifying Proteolytically Active Venom Toxins Using Fluorescently Labeled Substrates.
993 Biology (Basel). 2023;12(6).

994 63. Evans JD, Stark A, Johnson CD, Daniel F, Carmichael J, Buckels J, et al. A phase II trial
995 of marimastat in advanced pancreatic cancer. Br J Cancer. 2001 Dec 11;85(12):1865–70.

996 64. Quirt I, Bodurtha A, Lohmann R, Rusthoven J, Belanger K, Young V, et al. Phase II study
997 of marimastat (BB-2516) in malignant melanoma: A clinical and tumor biopsy study of

the National Cancer Institute of Canada Clinical Trials Group. Invest New Drugs. 2002 Nov;20(4):431–7.

65. Franken H, Mathieson T, Childs D, Sweetman GMA, Werner T, Tögel I, et al. Thermal proteome profiling for unbiased identification of direct and indirect drug targets using multiplexed quantitative mass spectrometry. Nat Protoc. 2015 Oct 29;10(10):1567–93.

66. Mateus A, Kurzawa N, Becher I, Sridharan S, Helm D, Stein F, et al. Thermal proteome profiling for interrogating protein interactions. Mol Syst Biol. 2020 Mar 5;16(3):9232.

67. Van Vranken JG, Li J, Mitchell DC, Navarrete-Perea J, Gygi SP. Assessing target engagement using proteome-wide solvent shift assays. Elife. 2021;10.

68. Zhang X, Wang Q, Li Y, Ruan C, Wang S, Hu L, et al. Solvent-Induced Protein Precipitation for Drug Target Discovery on the Proteomic Scale. Anal Chem. 2020;92(1).

69. Mateus A, Määttä TA, Savitski MM. Thermal proteome profiling: Unbiased assessment of protein state through heat-induced stability changes. Proteome Science BioMed Central Ltd.; Jun 24, 2017 p. 1–7.

70. Gaetani M, Sabatier P, Saei AA, Beusch CM, Yang Z, Lundström SL, et al. Proteome Integral Solubility Alteration: A High-Throughput Proteomics Assay for Target Deconvolution. J Proteome Res. 2019;18(11).

71. Gaetani M, Zubarev RA. Proteome Integral Solubility Alteration (PISA) for High-Throughput Ligand Target Deconvolution with Increased Statistical Significance and Reduced Sample Amount. Methods Mol Biol. 2023;2554:91–106.

1018 72. Zhang X, Lytovchenko O, Lundström S, Zubarev R, Gaetani M. Proteome Integral
1019 Solubility Alteration (PISA) Assay in Mammalian Cells for Deep, High-Confidence, and
1020 High-Throughput Target Deconvolution. Bio-protocol. 2022 Nov 20;12(22):e4556–e4556.

1021 73. Li J, Van Vranken JG, Paulo JA, Huttlin EL, Gygi SP. Selection of Heating Temperatures
1022 Improves the Sensitivity of the Proteome Integral Solubility Alteration Assay. J Proteome
1023 Res. 2020;19(5):2159–66.

1024 74. Savitski MM, Reinhard FBM, Franken H, Werner T, Savitski MF, Eberhard D, et al.
1025 Tracking cancer drugs in living cells by thermal profiling of the proteome. Science (80-).
1026 2014 Oct 3;346(6205).

1027 75. Peng H, Guo H, Pogoutse O, Wan C, Hu LZ, Ni Z, et al. An Unbiased Chemical
1028 Proteomics Method Identifies FabI as the Primary Target of 6-OH-BDE-47. Environ Sci
1029 Technol. 2016 Oct 18;50(20):11329–36.

1030 76. Ruan C, Ning W, Liu Z, Zhang X, Fang Z, Li Y, et al. Precipitate-Supported Thermal
1031 Proteome Profiling Coupled with Deep Learning for Comprehensive Screening of Drug
1032 Target Proteins. ACS Chem Biol. 2022;17(1).

1033 77. Modahl CM, Mrinalini, Frietze S, Mackessy SP. Adaptive evolution of distinct prey-
1034 specific toxin genes in rear-fanged snake venom. Proc R Soc B Biol Sci. 2018;285(1884).

1035 78. Modahl CM, Frietze S, Mackessy SP. Transcriptome-facilitated proteomic
1036 characterization of rear-fanged snake venoms reveal abundant metalloproteinases with
1037 enhanced activity. J Proteomics. 2018;187:223–34.

1038 79. Bolger AM, Lohse M, Usadel B. Trimmomatic: A flexible trimmer for Illumina sequence
1039 data. Bioinformatics. 2014;30(15):2114–20.

1040 80. Langmead B, Salzberg SL. Fast gapped-read alignment with Bowtie 2. Nat Methods.
1041 2012;9(4):357–9.

1042 81. Dowell NL, Giorgianni MW, Kassner VA, Selegue JE, Sanchez EE, Carroll SB. The deep
1043 origin and recent loss of venom toxin genes in rattlesnakes. Curr Biol. 2016;26(18):2434–
1044 45.

1045 82. Rokyta DR, Lemmon AR, Margres MJ, Aronow K. The venom-gland transcriptome of the
1046 eastern diamondback rattlesnake (*Crotalus adamanteus*). BMC Genomics. 2012;13(1).

1047 83. McGivern JJ, Wray KP, Margres MJ, Couch ME, Mackessy SP, Rokyta DR. RNA-seq
1048 and high-definition mass spectrometry reveal the complex and divergent venoms of two
1049 rear-fanged colubrid snakes. BMC Genomics. 2014 Dec 3;15(1):1–18.

1050 84. Zhang J, Kobert K, Flouri T, Stamatakis A. PEAR: A fast and accurate Illumina Paired-
1051 End reAd mergeR. Bioinformatics. 2014;30(5):614–20.

1052 85. Archer J, Whiteley G, Casewell NR, Harrison RA, Wagstaff SC. VTBuilder: A tool for
1053 the assembly of multi isoform transcriptomes. BMC Bioinformatics. 2014;15(1).

1054 86. Gilbert DG. Gene-omes built from mRNA-seq not genome DNA. 7th Annu Arthropod
1055 Genomics Symp. 2013;47405.

1056 87. Li W, Godzik A. Cd-hit: A fast program for clustering and comparing large sets of protein
1057 or nucleotide sequences. Bioinformatics. 2006;22(13):1658–9.

1058 88. Fu L, Niu B, Zhu Z, Wu S, Li W. CD-HIT: Accelerated for clustering the next-generation
1059 sequencing data. Bioinformatics. 2012;28(23):3150–2.

1060 89. Li B, Dewey CN. RSEM: Accurate transcript quantification from RNA-Seq data with or
1061 without a reference genome. BMC Bioinformatics. 2011;12.

1062 90. Buchfink B, Xie C, Huson DH. Fast and sensitive protein alignment using DIAMOND.
1063 Nat Methods. 2014;12(1):59–60.

1064 91. Nachtigall PG, Rautsaw RM, Ellsworth SA, Mason AJ, Rokyta DR, Parkinson CL, et al.
1065 ToxCodAn: A new toxin annotator and guide to venom gland transcriptomics. Brief
1066 Bioinform. 2021;22(5).

1067 92. Jarzab A, Kurzawa N, Hopf T, Moerch M, Zecha J, Leijten N, et al. Meltome atlas—
1068 thermal proteome stability across the tree of life. Nat Methods. 2020;17(5):495–503.

1069 93. Smith CF, Mackessy SP. The effects of hybridization on divergent venom phenotypes:
1070 Characterization of venom from *Crotalus scutulatus scutulatus* × *Crotalus oreganus*
1071 *helleri* hybrids. Toxicon. 2016;120:110–23.

1072 94. Dzieciatkowska M, Hill R, Hansen KC. GeLC-MS/MS analysis of complex protein
1073 mixtures. Methods Mol Biol. 2014;1156:53–66.

1074 95. Calvete JJ, Fasoli E, Sanz L, Boschetti E, Righetti PG. Exploring the venom proteome of
1075 the western diamondback rattlesnake, Crotalus atrox, via snake venomics and
1076 combinatorial peptide ligand library approaches. J Proteome Res. 2009 Jun 5;8(6):3055–
1077 67.

1078 96. Yu F, Teo GC, Kong AT, Haynes SE, Avtonomov DM, Geiszler DJ, et al. Identification
1079 of modified peptides using localization-aware open search. Nat Commun. 2020;11(1):1–9.

1080 97. Kong AT, Leprevost F V, Avtonomov DM, Mellacheruvu D, Nesvizhskii AI. MSFragger:
1081 Ultrafast and comprehensive peptide identification in mass spectrometry-based
1082 proteomics. Nat Methods. 2017;14(5):513–20.

1083 98. Zhu W, Smith JW, Huang CM. Mass spectrometry-based label-free quantitative
1084 proteomics. J Biomed Biotechnol. 2010;2010:840518.

1085 99. Ji H, Lu X, Zheng Z, Sun S, Tan CSH. ProSAP: a GUI software tool for statistical
1086 analysis and assessment of thermal stability data. Brief Bioinform. 2022 May 13;23(3).

1087 100. Giorgianni MW, Dowell NL, Griffin S, Kassner VA, Selegue JE, Carroll SB. The origin
1088 and diversification of a novel protein family in venomous snakes. Proc Natl Acad Sci U S
1089 A. 2020 May 19;117(20):10911–20.

1090 101. Harrison RA, Oluoch GO, Ainsworth S, Alsolaiss J, Bolton F, Arias AS, et al. Preclinical
1091 antivenom-efficacy testing reveals potentially disturbing deficiencies of snakebite
1092 treatment capability in East Africa. PLoS Negl Trop Dis. 2017;11(10).

1093 102. Lewin MR, Carter RW, Matteo IA, Samuel SP, Rao S, Fry BG, et al. Varespladib in the
1094 Treatment of Snakebite Envenoming: Development History and Preclinical Evidence
1095 Supporting Advancement to Clinical Trials in Patients Bitten by Venomous Snakes.
1096 Toxins (Basel). 2022;14(11).

1097 103. Abouyannis M, FitzGerald R, Ngama M, Mwangudzah H, Nyambura YK, Ngome S, et al.

TRUE-1: Trial of Repurposed Unithiol for snakebite Envenoming phase 1 (safety, tolerability, pharmacokinetics and pharmacodynamics in healthy Kenyan adults). Wellcome Open Res. 2022;7.

104. Lewin M, Samuel S, Merkel J, Bickler P. Varespladib (LY315920) appears to be a potent, broad-spectrum, inhibitor of snake venom phospholipase A2 and a possible pre-referral treatment for envenomation. Toxins (Basel). 2016;8(9).

105. Bryan-Quirós W, Fernández J, Gutiérrez JM, Lewin MR, Lomonte B. Neutralizing properties of LY315920 toward snake venom group I and II myotoxic phospholipases A2. Toxicon. 2019;157:1–7.

106. Xie C, Albulescu LO, Still KBM, Slagboom J, Zhao Y, Jiang Z, et al. Varespladib inhibits the phospholipase A2 and coagulopathic activities of venom components from hemotoxic snakes. Biomedicines. 2020;8(6):1–17.

107. Youngman NJ, Walker A, Naude A, Coster K, Sundman E, Fry BG. Varespladib (LY315920) neutralises phospholipase A2 mediated prothrombinase-inhibition induced by Bitis snake venoms. Comp Biochem Physiol Part - C Toxicol Pharmacol. 2020;236.

108. Dashevsky D, Bénard-Valle M, Neri-Castro E, Youngman NJ, Zdenek CN, Alagón A, et al. Anticoagulant Micrurus venoms: Targets and neutralization. Toxicol Lett. 2021;337:91–7.

109. Molina DM, Jafari R, Ignatushchenko M, Seki T, Larsson EA, Dan C, et al. Monitoring drug target engagement in cells and tissues using the cellular thermal shift assay. Science (80-). 2013 Jul 5;341(6141):84–7.

110. Albulescu LO, Hale MS, Ainsworth S, Alsolaiss J, Crittenden E, Calvete JJ, et al. Preclinical validation of a repurposed metal chelator as an early-intervention therapeutic for hemotoxic snakebite. Sci Transl Med. 2020 May 6;12(542).

111. Panecka-Hofman J, Pöhner I, Spyrakis F, Zeppelin T, Di Pisa F, Dello Iacono L, et al. Comparative mapping of on-targets and off-targets for the discovery of anti-trypanosomatid folate pathway inhibitors. Biochim Biophys Acta - Gen Subj. 2017 Dec 1;1861(12):3215–30.

112. Dwivedi AK, Gurjar V, Kumar S, Singh N. Molecular basis for nonspecificity of nonsteroidal anti-inflammatory drugs (NSAIDs). Drug Discov Today. 2015;20(7):863–73.

113. Montecucco C, Gutiérrez JM, Lomonte B. Cellular pathology induced by snake venom phospholipase A2 myotoxins and neurotoxins: Common aspects of their mechanisms of action. Vol. 65, Cellular and Molecular Life Sciences. 2008. p. 2897–912.

114. Shashidharamurthy R, Kemparaju K. A neurotoxic phospholipase A2 variant: Isolation and characterization from eastern regional Indian cobra (Naja naja) venom. Toxicon. 2006;

115. Xiao H, Li H, Zhang D, Li Y, Sun S, Huang C. Inactivation of venom PLA2 alleviates myonecrosis and facilitates muscle regeneration in envenomed mice: A time course observation. Molecules. 2018;23(8).

116. Moura-da-Silva AM, Almeida MT, Portes-Junior JA, Nicolau CA, Gomes-Neto F, Valente RH. Processing of snake venom metalloproteinases: Generation of toxin diversity and enzyme inactivation. Vol. 8, Toxins. 2016.

1140 117. Deshimaru M, Ogawa T, Nakashima K ichi, Nobuhisa I, Chijiwa T, Shimohigashi Y, et al.
1141 Accelerated evolution of crotalinae snake venom gland serine proteases. FEBS Lett. 1996
1142 Nov 11;397(1):83–8.

1143 118. Kini RM, Chan YM. Accelerated evolution and molecular surface of venom
1144 phospholipase A2 enzymes. J Mol Evol. 1999;48(2).

1145 119. Lynch VJ. Inventing an arsenal: Adaptive evolution and neofunctionalization of snake
1146 venom phospholipase A2 genes. BMC Evol Biol. 2007;7.

1147 120. Kini RM. Evolution of three-finger toxins - A versatile mini protein scaffold. Acta Chim
1148 Slov. 2011;58(4):693–701.

1149 121. Sunagar K, Fry BG, Jackson TNW, Casewell NR, Undheim EAB, Vidal N, et al.
1150 Molecular evolution of vertebrate neurotrophins: Co-option of the highly conserved nerve
1151 growth factor gene into the advanced snake venom arsenalf. PLoS One. 2013 Nov
1152 29;8(11):e81827.

1153 122. Lomonte B, Calvete JJ. Strategies in ‘snake venomics’ aiming at an integrative view of
1154 compositional, functional, and immunological characteristics of venoms. J Venom Anim
1155 Toxins Incl Trop Dis. 2017 Apr 28;23(1).

1156 123. Slagboom J, Kaal C, Arrahman A, Vonk FJ, Somsen GW, Calvete JJ, et al. Analytical
1157 strategies in venomics. Microchem J. 2022;175.

1158 124. Lauridsen LP, Laustsen AH, Lomonte B, Gutiérrez JM. Exploring the venom of the forest
1159 cobra snake: Toxicovenomics and antivenom profiling of Naja melanoleuca. J Proteomics.

2017;

125. Calvete JJ, Lomonte B, Saviola AJ, Bonilla F, Sasa M, Williams DJ, et al. Mutual enlightenment: A toolbox of concepts and methods for integrating evolutionary and clinical toxinology via snake venomics and the contextual stance. Toxicon X. 2021 Jul 1;9–10:100070.

Figure Legends

Figure 1. TPP (a) and PISA (b) workflows. a) In TPP experiments, samples are heated between 40 – 70°C and centrifuged to pellet denatured proteins. Samples are reduced, alkylated, and trypsin digested and analyzed with LC-MS/MS for protein identification. Melting curves are generated in ProSAP using unique intensity for each protein identified. T_m = melting temperature of 50% of population. b) In PISA, venom is incubated for 30 minutes at 37°C with an inhibitor or alone. Samples are heated from 40-70°C, and pooled before centrifuging to pellet insoluble material. Samples are prepared as mentioned above and analyzed via LC-MS/MS for protein identification. To identify inhibitor targets, unique intensity is used to calculate SAR values for each protein followed by identification of significant outliers.

Figure 2. *Crotalus atrox* venom proteome characterization. a) Toxin family abundances in *C. atrox* venom modified from Calvete et al., 2009. b) The number of proteoforms identified in *C. atrox* venom in the present study organized by family. c) RP-HPLC separated *C. atrox* venom. For peak identification fractions were analyzed with mass spectrometry and SDS-PAGE and compared to known masses from Calvete et al., 2009. SVMP=Snake venom metalloprotease, CTL=C-type lectin, SVSP=snake venom serine protease, Dis=disintegrin, PLA_2 =phospholipase A_2, BPP=Bradykinin potentiating peptide, CRISP=cysteine rich secretory protein, L-AAO=L-amino acid oxidase, SVMPi= SVMP tripeptide inhibitor, PLB= Phospholipase B, NGF=nerve growth factor, HYAL=hyaluronidase, GPC=glutaminyl-peptide cyclotransferase, VEGF=vascular endothelial growth factor.

Figure 3. *C. atrox* meltome characterization. a) SDS-PAGE of *C. atrox* venom heated at temperatures between 37-70°C for 3 minutes. b) Heatmap showing the thermal denaturation of

most toxin proteoforms across 10 temperatures where 37°C represents the nondenatured control. Heatmap colors represent normalized intensity and are scaled by row to better visualize variation in intensity between temperatures. c) Distribution of melting temperatures organized by family. Dotted lines represent median and quartile ranges. d) Distribution of melting temperatures for all toxins identified. Nonmelters (NM) are classified as proteoforms for which T_m could not be calculated when heated to a maximum temperature of 75°C. e) Representative melting curve of a CTL (Crotocetin). Abundance is normalized to 37°C f) Representative melting curve of a PLA_2 (Cvv-N6). Abundance is normalized to 37°C. g) Representative melting curve of an SVMP (PIII 28325). Abundance is normalized to 37°C.

Figure 4. *C. atrox* venom-wide interactions with two concentrations of marimastat with temperature window from 40-70°C. a) Volcano plot comparing soluble supernatant of heat-treated venom + marimastat (15 μM) to heat-treated venom alone. X indicates SVMP proteoforms, red=positive outliers, blue=negative outliers, grey=not significant. b) Volcano plot comparing soluble supernatant of heat-treated venom + marimastat (150 μM) to heat-treated venom alone. c) Volcano plot comparing insoluble precipitate of heat-treated venom + marimastat (15 μM) to heat-treated venom alone. d) Volcano plot comparing insoluble precipitate of heat-treated venom + marimastat (150 μM) to heat-treated venom alone.

Figure 5. Validation assays of inhibitor interactions. a) SDS-PAGE comparison of heat-treated venom to heat-treated venoms incubated with 150 μM of marimastat with a thermal window of 40-70°C. Note the recovery in band size and intensity of SVMP and PLA_2 bands in marimastat-treated samples. Left side indicates molecular mass standards in kDa. b) Enlarged HPLC-separated SVMP peak overlay comparing abundance of non-heat-treated venom (black), heat-treated venom (red), and venom heat-treated after incubation with 150 μM of marimastat (blue).

Note the recovery of peak area in the inhibitor-treated sample. c) Enlarged HPLC-separated PLA_2 peak overlay comparing abundance of non-heat-treated venom (black), heat-treated venom (red), and venom heat-treated after incubation with 150 μM of marimastat (blue). Note the recovery of PLA_2 peak area in the inhibitor-treated sample.

Figure 6. *C. atrox* venom-wide interactions with two concentrations of marimastat with temperature window from 56-60°C. a) Volcano plot comparing soluble supernatant of heat-treated venom + marimastat (15 μM) to heat-treated venom alone. X indicates SVMP proteoforms, red=positive outliers, blue=negative outliers, grey=not significant. b) Volcano plot comparing soluble supernatant of heat-treated venom + marimastat (150 μM) to heat-treated venom alone. c) Volcano plot comparing insoluble precipitate of heat-treated venom + marimastat (15 μM) to heat-treated venom alone. d) Volcano plot comparing insoluble precipitate of heat-treated venom + marimastat (150 μM) to heat-treated venom alone.

Figure 7. Comparison of a broad (40-70°C) to a narrow (56-60°C) PISA thermal window. PCA plot comparing replicates of soluble supernatant of a) heat-treated venom + 15 μM marimastat to heat-treated venom alone and b) heat-treated venom + 150 μM marimastat to heat-treated venom alone. SN= supernatant, Pell= pellet, Con= control. PCA plot with 95% confidence intervals comparing replicates of insoluble precipitate of c) heat-treated venom + 15 μM marimastat to heat-treated venom alone and d) heat-treated venom + 150 μM marimastat to heat-treated venom alone. SN= supernatant, Pell=pellet. SN= supernatant, Pell= pellet, Con= control. e) Number of SVMP and non-SVMP proteins identified with significant thermal shifts toward stabilization (p-value<0.05 $\log_2$SAR>0.5) after 15 μM or 150 μM marimastat treatment in supernatants and pellets heat-treated at a broad (40-70°C) or a narrow (56-60°C) thermal window. SN=supernatant, P=pellet. Venn diagrams of SVMP proteins identified with significant thermal

shifts toward stabilization (p-value<0.05, log_2SAR>0.5) in supernatants and pellets heat-treated at a broad (40-70°C) or a narrow (56-60°C) thermal window after f) 15 μM or g) 150 μM marimastat treatment. SN= supernatant, Pell=pellet. Scatter plot showing log_2SAR values calculated from 150 μM marimastat-treated venom vs. vehicle treatment heated at from h) 40-70°C or i) 56-60°C that meet significance criteria in both supernatant (SN) and precipitate (Pellet) group. Largest outliers of SVMP and non-SVMP proteoforms are labeled. SN=supernatant. Black=SVMP proteoforms, grey=non-SVMP toxins. SN= supernatant, Hyal=hyaluronidase, ACLD=PIII SVMP ACLD, CTL= C-type lectin.

Figure 8. Effects of marimastat treatment and a narrow thermal window on SVMP proteoforms only. a) Number of proteins identified in supernatant (SN) and pellet of narrow thermal window that meet significance criteria (p-value<0.01, log_2SAR>0.5) b) heatmap of sum-normalized intensity values in supernatant or precipitate of SVMPs from 15 μM or 150 μM marimastat treated venom. Heatmap colors are scaled by row to better visualize variation in sum-normalized intensity between classes. c) heatmap of sum-normalized intensity values in supernatant or precipitate of SVMPs from 15 μM or 150 μM marimastat treated venom or vehicle control showing concentration-dependent shifts in abundance. Heatmap colors are scaled by row to better visualize variation in sum-normalized intensity between classes. d) Correlation plot of SAR values showing strongest marimastat targets based on effects of marimastat treatment on SVMP proteoform intensity. Comparison of concentration-dependent intensity shifts between precipitate and supernatant of e) the most abundant SVMP proteoform VAP2B and f) a less abundant SVMP proteoform PIII 28348 at both concentrations of marimastat at the narrow thermal window.

Supplemental Material

Supplemental Figure 1. SDS-PAGE of reverse phase HPLC fractions from crude *C. atrox* venom.

Supplemental Table 1. Validation assay reverse phase HPLC fractions of crude untreated *C. atrox* venom and SDS-PAGE gel band protein identification with LC-MS/MS analysis.

Supplemental Table 2. Validation assay reverse phase HPLC fractions of marimastat-treated and untreated PISA samples.

Competing Interests

The authors declare no competing interests.

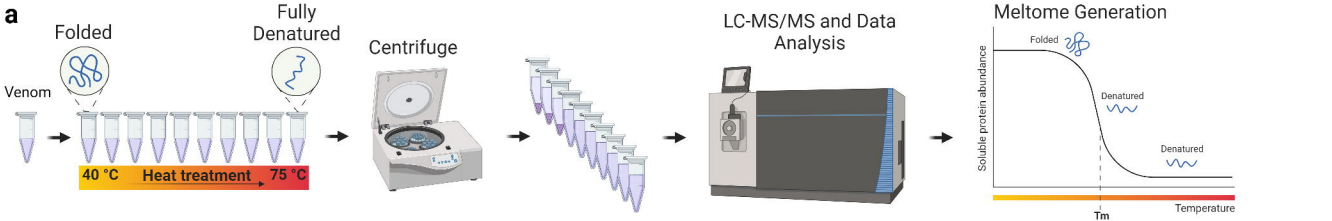
a
Folded
Fully Denatured
Venom
40 °C
Heat treatment
75 °C
Centrifuge
LC-MS/MS and Data Analysis
Meltome Generation
Folded
Denatured
Denatured
Soluble protein abundance
Tm
Temperature

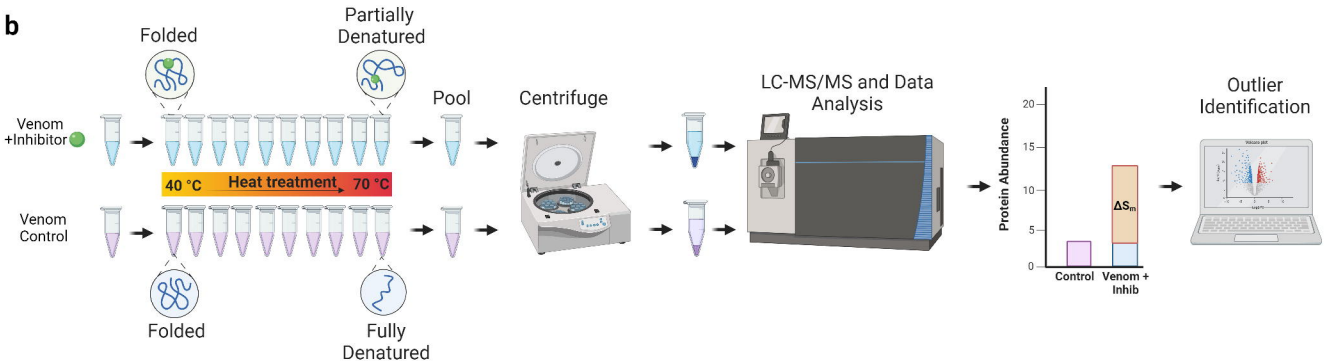
b
Folded
Partially Denatured
Venom +Inhibitor
40 °C
Heat treatment
70 °C
Venom Control
Pool
Centrifuge
LC-MS/MS and Data Analysis
Protein Abundance
20
15
10
5
0
ΔSm
Control
Venom + Inhib
Outlier Identification
Folded
Fully Denatured

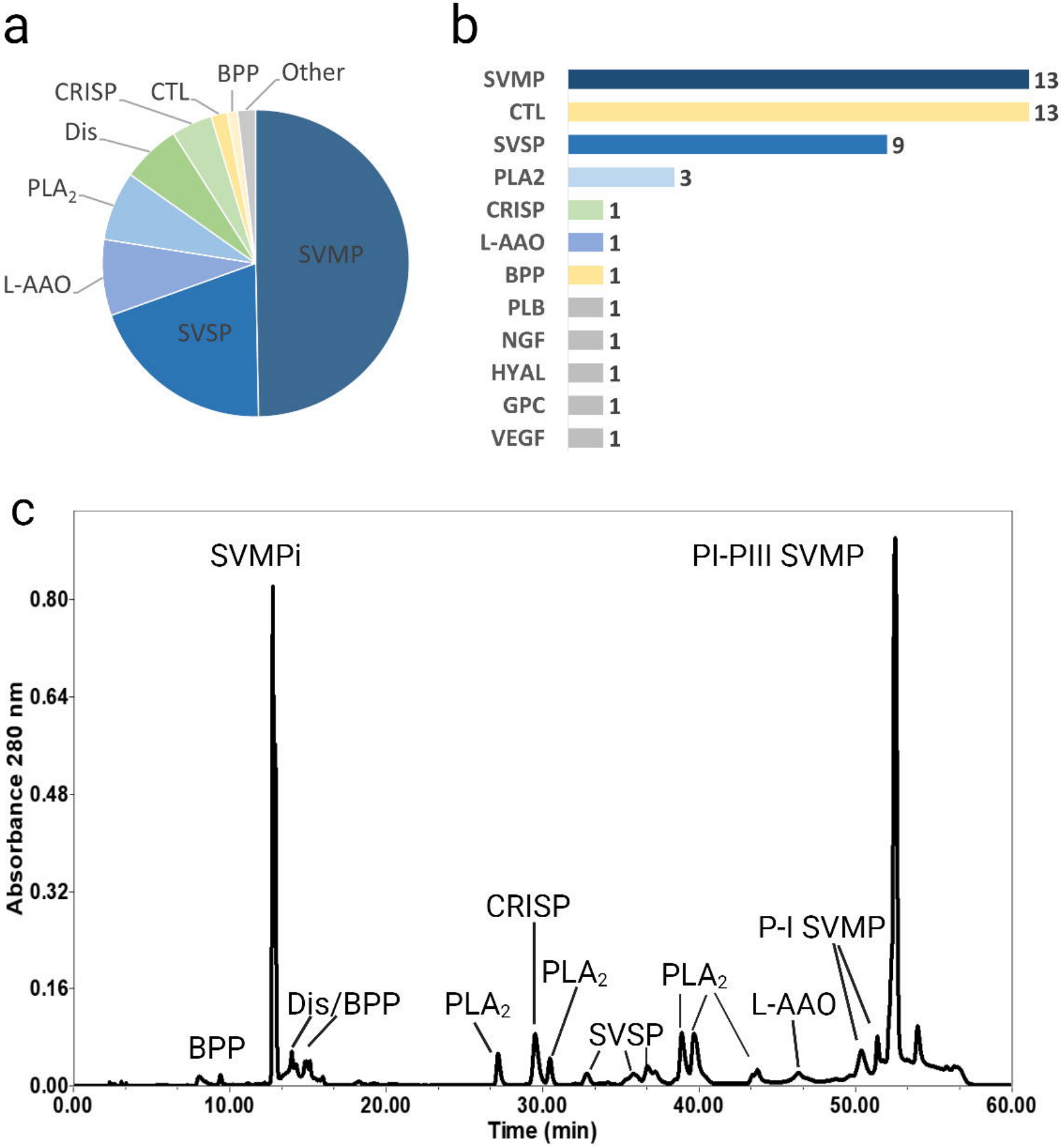
a
BPP
Other
CRISP
CTL
Dis
PLA2
L-AAO
SVMP
SVSP
b
SVMP 13
CTL 13
SVSP 9
PLA2 3
CRISP 1
L-AAO 1
BPP 1
PLB 1
NGF 1
HYAL 1
GPC 1
VEGF 1
c
SVMPi
PI-PIII SVMP
P-I SVMP
CRISP
PLA2
PLA2
PLA2
Dis/BPP
BPP
SVSP
L-AAO
Absorbance 280 nm
0.00
0.16
0.32
0.48
0.64
0.80
0.00
10.00
20.00
30.00
40.00
50.00
60.00
Time (min)

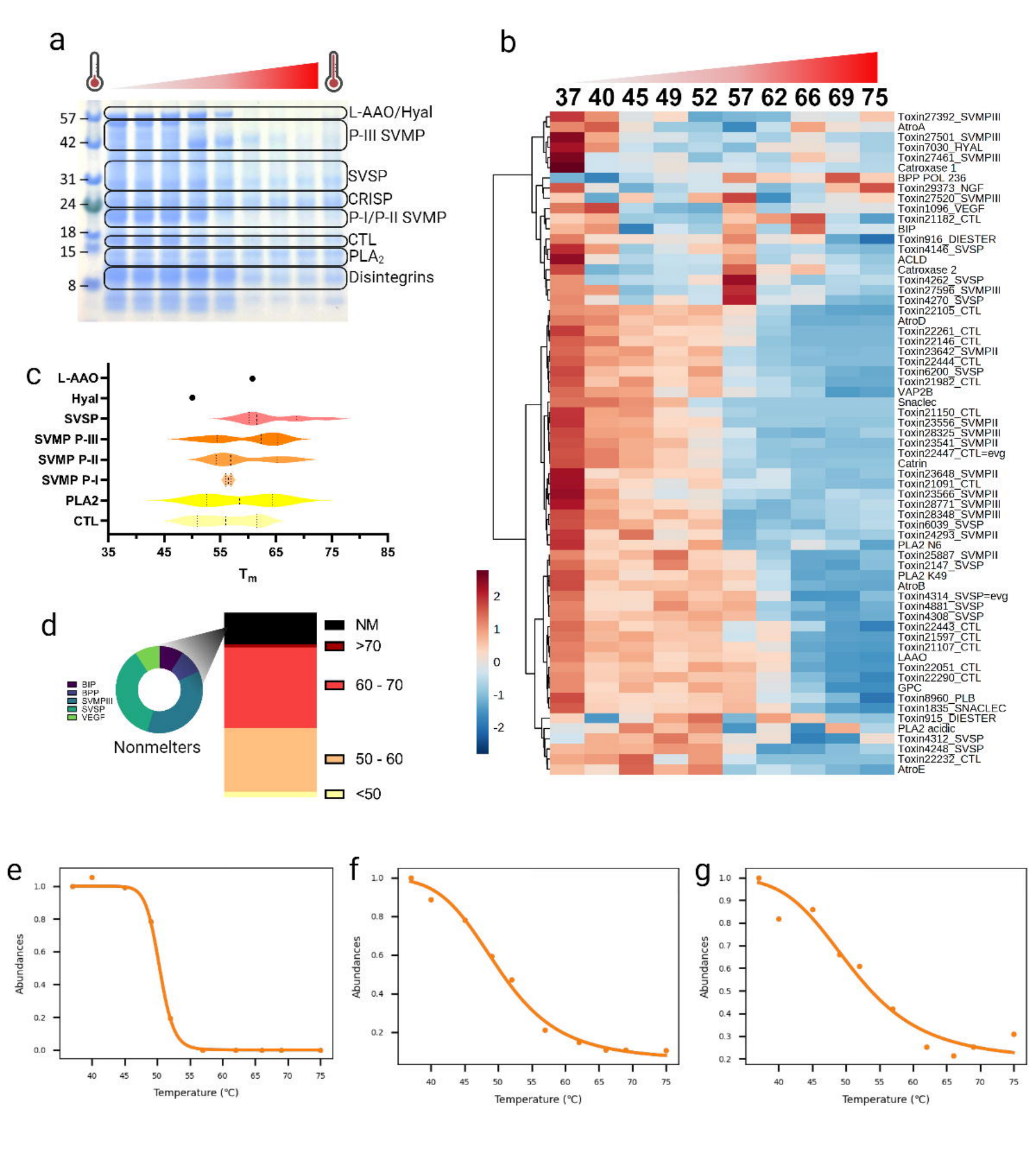
a
57
42
31
24
18
15
8
L-AAO/Hyal
P-III SVMP
SVSP
CRISP
P-I/P-II SVMP
CTL
PLA2
Disintegrins
b
37 40 45 49 52 57 62 66 69 75
Toxin27392_SVMPIII
AtroA
Toxin27501_SVMPIII
Toxin7030_HYAL
Toxin27461_SVMPIII
Catroxase 1
BPP POL 236
Toxin29373_NGF
Toxin27520_SVMPIII
Toxin1096_VEGF
Toxin21182_CTL
BIP
Toxin916_DIESTER
Toxin4146_SVSP
ACLD
Catroxase 2
Toxin4262_SVSP
Toxin27596_SVMPIII
Toxin4270_SVSP
Toxin22105_CTL
AtroD
Toxin22261_CTL
Toxin22146_CTL
Toxin23642_SVMPII
Toxin22444_CTL
Toxin6200_SVSP
Toxin21982_CTL
VAP2B
Snaclec
Toxin21150_CTL
Toxin23556_SVMPII
Toxin28325_SVMPIII
Toxin23541_SVMPII
Toxin22447_CTL=evg
Catrin
Toxin23648_SVMPII
Toxin21091_CTL
Toxin23566_SVMPII
Toxin28771_SVMPIII
Toxin28348_SVMPIII
Toxin6039_SVSP
Toxin24293_SVMPII
PLA2 N6
Toxin25887_SVMPII
Toxin2147_SVSP
PLA2 K49
AtroB
Toxin4314_SVSP=evg
Toxin4881_SVSP
Toxin4308_SVSP
Toxin22443_CTL
Toxin21597_CTL
Toxin21107_CTL
LAAO
Toxin22051_CTL
Toxin22290_CTL
GPC
Toxin8960_PLB
Toxin1835_SNACLEC
Toxin915_DIESTER
PLA2 acidic
Toxin4312_SVSP
Toxin4248_SVSP
Toxin22232_CTL
AtroE
2
1
0
-1
-2
c
L-AAO
Hyal
SVSP
SVMP P-III
SVMP P-II
SVMP P-I
PLA2
CTL
35 45 55 65 75 85
Tm
d
BIP
BPP
SVMPIII
SVSP
VEGF
Nonmelters
NM
>70
60 - 70
50 - 60
<50
e
Abundances
Temperature (°C)
f
Abundances
Temperature (°C)
g
Abundances
Temperature (°C)

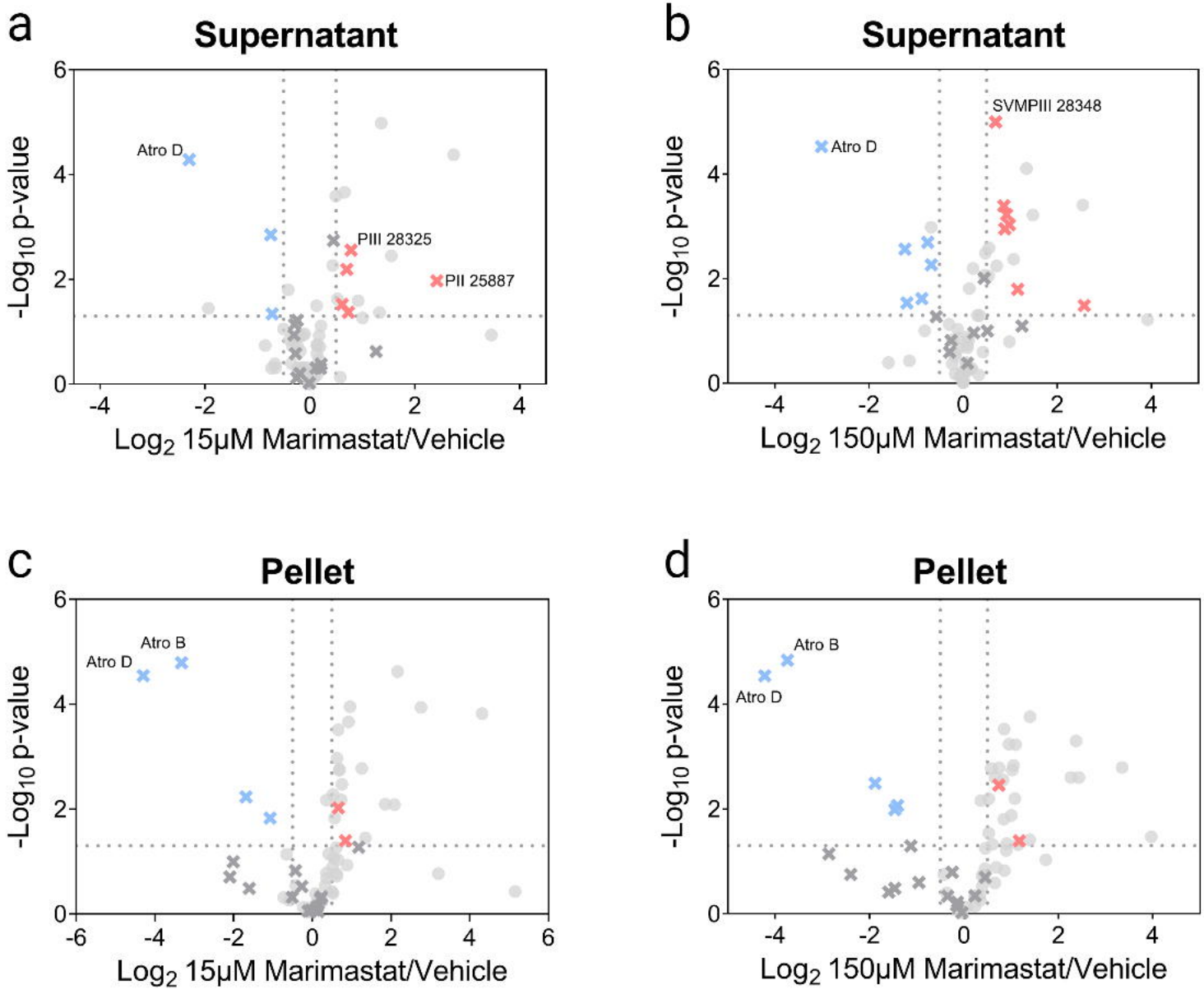
a
Supernatant
Atro D
PIII 28325
PII 25887
-Log10 p-value
Log2 15μM Marimastat/Vehicle
b
Supernatant
SVMPIII 28348
Atro D
-Log10 p-value
Log2 150μM Marimastat/Vehicle
c
Pellet
Atro B
Atro D
-Log10 p-value
Log2 15μM Marimastat/Vehicle
d
Pellet
Atro B
Atro D
-Log10 p-value
Log2 150μM Marimastat/Vehicle

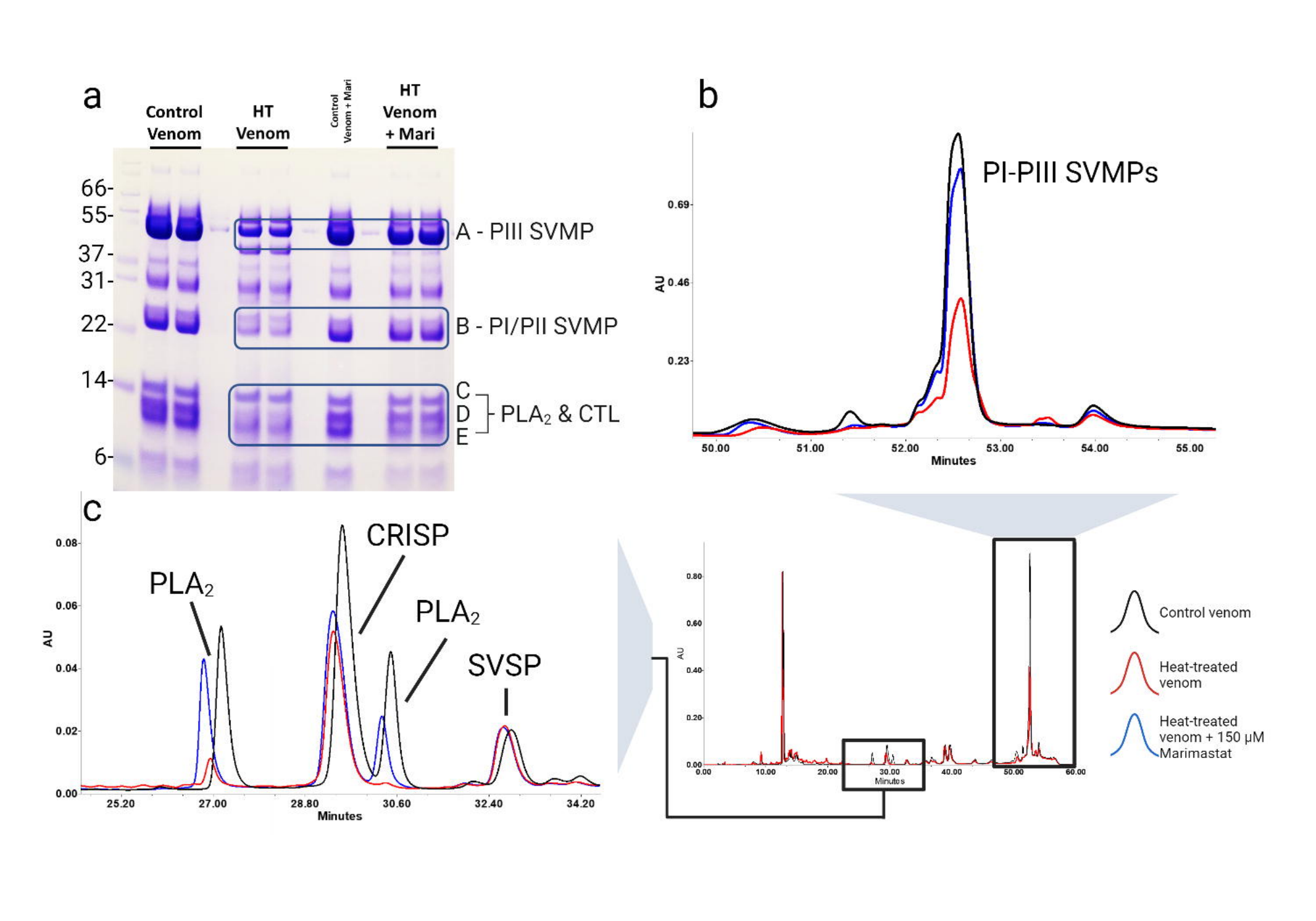
a
Control Venom
HT Venom
Control Venom + Mari
HT Venom + Mari
66-
55-
37-
31-
22-
14-
6-
A - PIII SVMP
B - PI/PII SVMP
C
D
E
PLA2 & CTL
b
PI-PIII SVMPs
AU
0.69
0.46
0.23
50.00
51.00
52.00
53.00
54.00
55.00
Minutes
c
AU
0.08
0.06
0.04
0.02
0.00
PLA2
CRISP
PLA2
SVSP
25.20
27.00
28.80
30.60
32.40
34.20
Minutes
0.80
0.60
0.40
0.20
0.00
0.00
10.00
20.00
30.00
40.00
50.00
60.00
Minutes
Control venom
Heat-treated venom
Heat-treated venom + 150 µM Marimastat

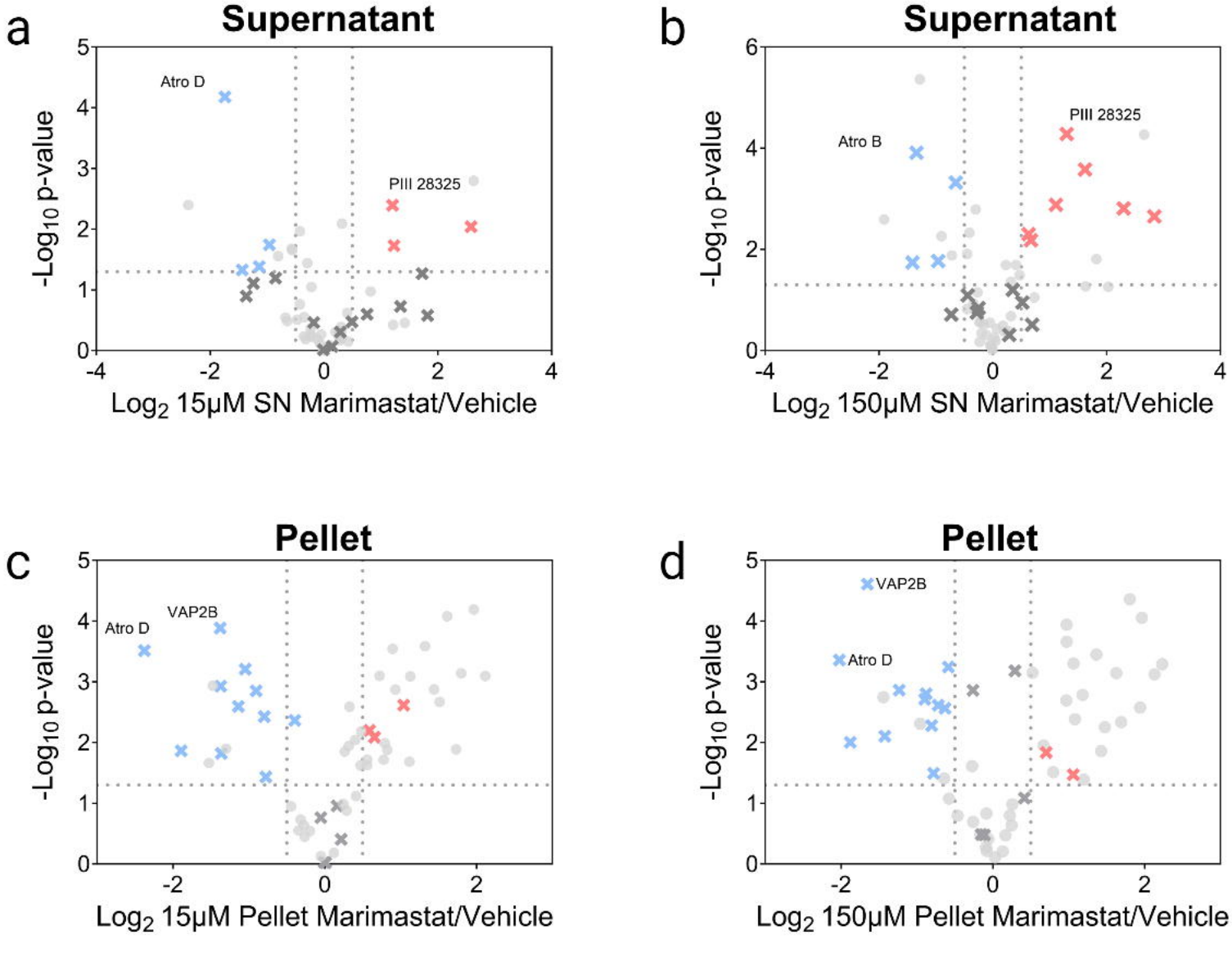
a
Supernatant
Atro D
PIII 28325
-Log10 p-value
Log2 15μM SN Marimastat/Vehicle
b
Supernatant
Atro B
PIII 28325
-Log10 p-value
Log2 150μM SN Marimastat/Vehicle
c
Pellet
VAP2B
Atro D
-Log10 p-value
Log2 15μM Pellet Marimastat/Vehicle
d
Pellet
VAP2B
Atro D
-Log10 p-value
Log2 150μM Pellet Marimastat/Vehicle

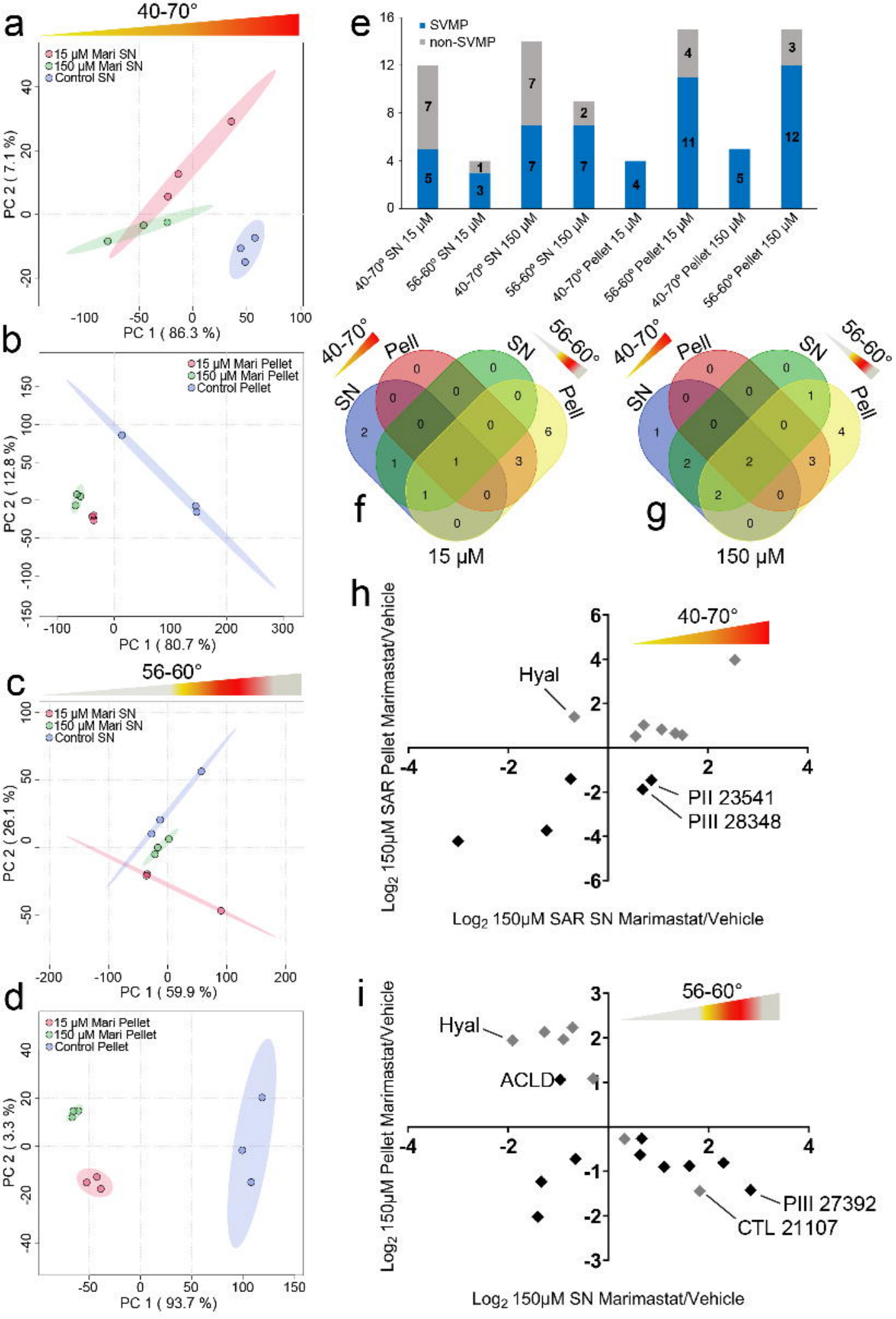
a
40-70°
15 µM Mari SN
150 µM Mari SN
Control SN
PC 2 (7.1 %)
PC 1 (86.3 %)
b
15 µM Mari Pellet
150 µM Mari Pellet
Control Pellet
PC 2 (12.8 %)
PC 1 (80.7 %)
c
56-60°
15 µM Mari SN
150 µM Mari SN
Control SN
PC 2 (26.1 %)
PC 1 (59.9 %)
d
15 µM Mari Pellet
150 µM Mari Pellet
Control Pellet
PC 2 (3.3 %)
PC 1 (93.7 %)
e
SVMP
non-SVMP
40-70° SN 15 µM
56-60° SN 15 µM
40-70° SN 150 µM
56-60° SN 150 µM
40-70° Pellet 15 µM
56-60° Pellet 15 µM
40-70° Pellet 150 µM
56-60° Pellet 150 µM
f
15 µM
g
150 µM
Pell
SN
h
Hyal
PII 23541
PIII 28348
Log2 150µM SAR Pellet Marimastat/Vehicle
Log2 150µM SAR SN Marimastat/Vehicle
i
ACLD
PIII 27392
CTL 21107
Log2 150µM Pellet Marimastat/Vehicle
Log2 150µM SN Marimastat/Vehicle

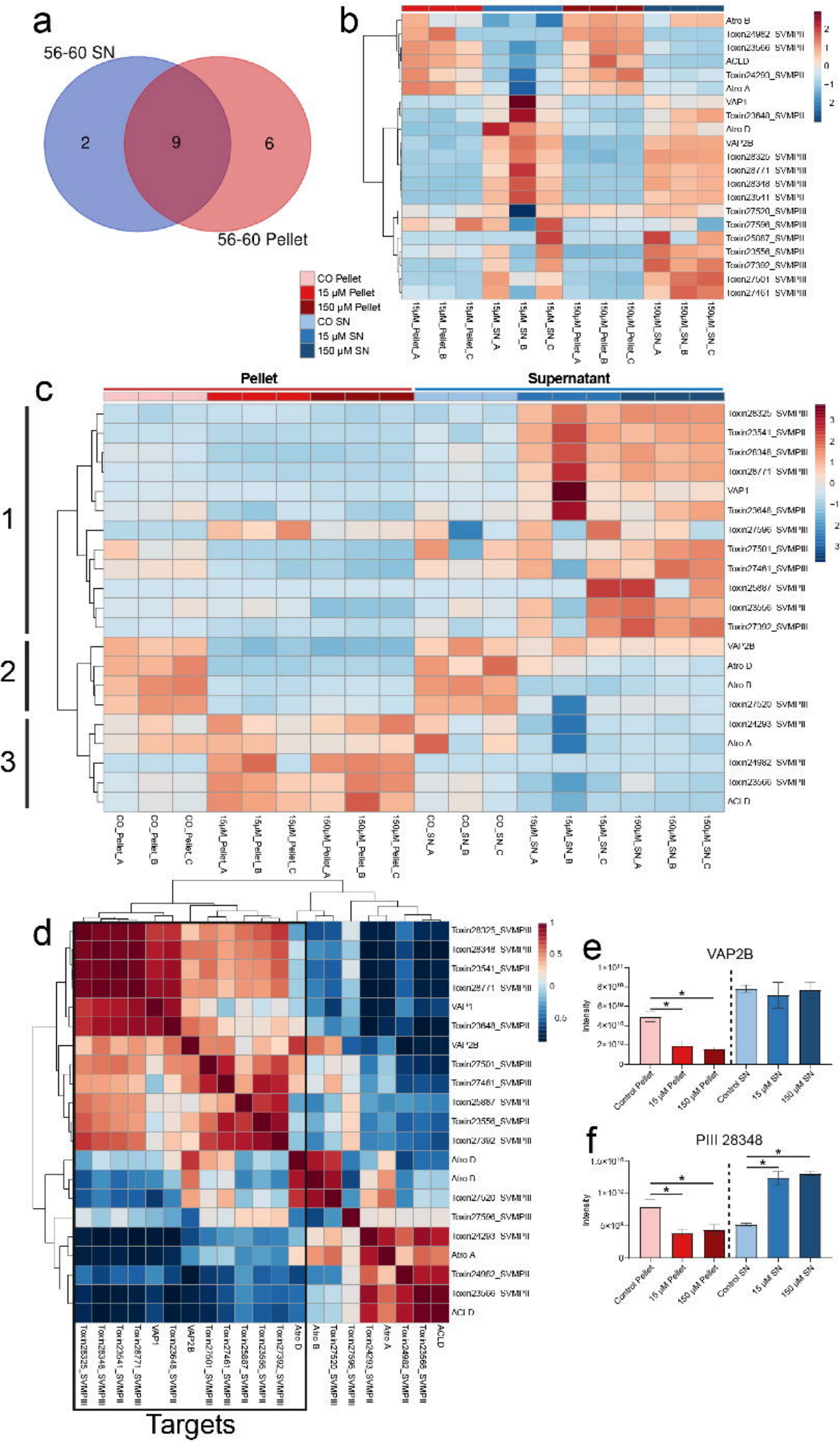
a
56-60 SN
2
9
6
56-60 Pellet
b
Atro B
Toxin24982_SVMPIII
Toxin23566_SVMPIII
ACLD
Toxin24293_SVMPIII
Atro A
VAP1
Toxin23648_SVMPII
Atro D
VAP2B
Toxin28325_SVMPIII
Toxin28771_SVMPIII
Toxin28348_SVMPIII
Toxin23541_SVMPII
Toxin27520_SVMPIII
Toxin27596_SVMPIII
Toxin25887_SVMPII
Toxin23556_SVMPII
Toxin27392_SVMPIII
Toxin27501_SVMPIII
Toxin27461_SVMPIII
CO Pellet
15 μM Pellet
150 μM Pellet
CO SN
15 μM SN
150 μM SN
15μM_Pellet_A
15μM_Pellet_B
15μM_Pellet_C
15μM_SN_A
15μM_SN_B
15μM_SN_C
150μM_Pellet_A
150μM_Pellet_B
150μM_Pellet_C
150μM_SN_A
150μM_SN_B
150μM_SN_C
c
Pellet
Supernatant
1
2
3
d
Targets
e
VAP2B
Intensity
Control Pellet
15 μM Pellet
150 μM Pellet
Control SN
15 μM SN
150 μM SN
f
PIII 28348
Intensity
Control Pellet
15 μM Pellet
150 μM Pellet
Control SN
15 μM SN
150 μM SN